CellPress
Partner Journal

Molecular Plant
Research Article

Regulation of floral senescence in *Arabidopsis* by coordinated action of *CONSTANS* and jasmonate signaling

Gloria Serrano-Bueno[1,5,*], Pedro de los Reyes[1,5], Andrea Chini[2], Gabriel Ferreras-Garrucho[1,3], Víctor Sánchez de Medina-Hernández[1,4], Marta Boter[2], Roberto Solano[2] and Federico Valverde[1,*]

[1]Plant Development Group, Institute for Plant Biochemistry and Photosynthesis, CSIC-Universidad de Sevilla, 41092 Sevilla, Spain

[2]Department of Plant Molecular Genetics, Centro Nacional de Biotecnología, CSIC, 28049 Madrid, Spain

[3]Present address: Crop Science Centre, University of Cambridge, Cambridge CB3 OLE Cambridge, UK

[4]Present address: Gregor Mendel Institute (GMI), Austrian Academy of Sciences, Vienna BioCenter (VBC), Vienna, Austria

[5]These authors contributed equally to this article.

***Correspondence: Gloria Serrano-Bueno (gloria.serrano@ibvf.csic.es), Federico Valverde (federico.valverde@ibvf.csic.es)**

https://doi.org/10.1016/j.molp.2022.09.017

ABSTRACT

In *Arabidopsis*, photoperiodic flowering is controlled by the regulatory hub gene *CONSTANS* (*CO*), whereas floral organ senescence is regulated by the jasmonates (JAs). Because these processes are chronologically ordered, it remains unknown whether there are common regulators of both processes. In this study, we discovered that CO protein accumulates in *Arabidopsis* flowers after floral induction, and it displays a diurnal pattern in floral organs different from that in the leaves. We observed that altered *CO* expression could affect flower senescence and abscission by interfering with JA response, as shown by petal-specific transcriptomic analysis as well as *CO* overexpression in JA synthesis and signaling mutants. We found that CO has a ZIM (ZINC-FINGER INFLORESCENCE MERISTEM) like domain that mediates its interaction with the JA response repressor JAZ3 (jasmonate ZIM-domain 3). Their interaction inhibits the repressor activity of JAZ3, resulting in activation of downstream transcription factors involved in promoting flower senescence. Furthermore, we showed that CO, JAZ3, and the E3 ubiquitin ligase COI1 (Coronatine Insensitive 1) could form a protein complex *in planta*, which promotes the degradation of both CO and JAZ3 in the presence of JAs. Taken together, our results indicate that CO, a key regulator of photoperiodic flowering, is also involved in promoting flower senescence and abscission by augmenting JA signaling and response. We propose that coordinated recruitment of photoperiodic and JA signaling pathways could be an efficient way for plants to chronologically order floral processes and ensure the success of offspring production.

Key words: CONSTANS, flower senescence, jasmonic acid

Serrano-Bueno G., de los Reyes P., Chini A., Ferreras-Garrucho G., Sánchez de Medina-Hernández V., Boter M., Solano R., and Valverde F. (2022). Regulation of floral senescence in *Arabidopsis* by coordinated action of *CONSTANS* and jasmonate signaling. Mol. Plant. **15**, 1710–1724.

INTRODUCTION

The timing of flowering and senescence needs to be strictly governed to successfully complete the annual developmental program (Körner and Basler, 2010). Choosing the wrong time of the year to form a flower may be as deleterious for a plant as deciding the wrong moment to initiate flower senescence and fruit formation (Thomas, 2013). Although global warming tends to promote extreme changes in external cues that are harmful for plant development, the length of the day (photoperiod) is a solid signal on which the plant can reliably base crucial developmental decisions (Ettinger et al., 2021).

Published by the Molecular Plant Shanghai Editorial Office in association with Cell Press, an imprint of Elsevier Inc., on behalf of CSPB and CEMPS, CAS.

In the *Arabidopsis* photoperiodic flowering pathway, the BBX gene *CONSTANS* (*CO*) constitutes a hub that controls the expression of the florigen gene *FLOWERING LOCUS T* (*FT*) (Samach et al., 2000) in the leaf phloem (Andrés and Coupland, 2012). FT protein migrates to the emerging primordia to trigger the flowering process and eventual production of fruits (An et al., 2004). *CO* is controlled by the circadian clock at the mRNA level and by photoreceptors and ubiquitin ligases at the posttranslational level, resulting in fine-tuned regulation (Suárez-López et al., 2001; Valverde et al., 2004; Kinoshita and Richter, 2020). In *Arabidopsis* and other annual species, the coincidence of *CO* expression with its protein stability in the evening of an extended day ensures FT production at the optimal time that would maximize the success of the offspring (Austen et al., 2017). The photoperiod pathway is evolutionarily conserved from algae to higher plants and constitutes one of the earliest examples of developmental regulation in plants (Serrano-Bueno et al., 2017). Using the gene-regulatory network centered on *CO*, plants can impart day length information to key physiological processes other than floral transition, such as carbon metabolism (Ortiz-Marchena et al., 2014), stomatal opening (Ando et al., 2013), photoprotection (Gabilly et al., 2019; Tokutsu et al., 2019), and lipid metabolism (Deng et al., 2015).

Jasmonates (JAs) are lipid-derived phytohormones that regulate multiple stress responses (Kazan, 2015; Wasternack and Feussner, 2018). In addition, JAs are also involved in many developmental processes, including flower development and senescence (Howe et al., 2018; Wasternack and Feussner, 2018). Under basal conditions, JA-related transcription factors (TFs) are repressed by JAZ (JASMONATE-ZIM DOMAIN) repressors through their interaction with the adaptor protein NOVEL INTERACTOR OF JAZ, the transcriptional corepressor TOPLESS, and histone deacetylases, which contribute to locking chromatin in a silenced state. JAZ proteins also prevent recruitment of the MEDIATOR complex, which interacts with the general transcriptional machinery and is required for transcriptional activation (An et al., 2017; Howe et al., 2018; Zhai et al., 2020). Environmental stress as well as endogenous developmental processes induce accumulation of the bioactive form of the hormone (+)-7-iso-JA-Ile (JA-Ile) (Fonseca et al., 2009; Sheard et al., 2010). JA-Ile directly binds to the Coronatine Insensitive 1 (COI1)-JAZ coreceptor, triggering ubiquitination and degradation of the JAZ repressors and, therefore, releasing the TFs that finally activate JA responses (Chini et al., 2007, 2009, 2016; Maor et al., 2007; Thines et al., 2007; Saracco et al., 2009; Fernández-Calvo et al., 2011; Howe et al., 2018). Among the JAZ-repressed TFs, the master regulator MYC2 and other MYC family members (i.e., MYC3, MYC4, and MYC5) play a primary role in regulating most JA-mediated physiological responses (Lorenzo et al., 2004; Fernández-Calvo et al., 2011; Qi et al., 2015; Zander et al., 2020).

JAs are also important endogenous signals promoting leaf senescence. Senescent plants accumulate high levels of JA-Ile, leading to the activation of several TFs, including MYC2, MYC3, and MYC4, which, in turn, induce senescence-associated gene (*SAG*) expression by directly binding to their promoter regions (Qi et al., 2015; Hu et al., 2017; Howe et al., 2018). JAs also regulate several processes in flower development, such as stamen elongation, anther and pollen maturation, flower senescence, and flowering time (Mandaokar et al., 2006; Mandaokar and Browse, 2009; Song et al., 2011; Qi et al., 2015; Zhai et al., 2015; Acosta and Przybyl, 2019). Although the JA signaling pathway is highly redundant, specific components regulating discrete flower development processes have been identified (Chini et al., 2016; Howe et al., 2018). For example, JAZ repressors interact with pairs of TF activators, such as MYB21/MYB24 and TARGET OF EAT1 (TOE1)/TOE2 to control JA-mediated stamen development and flowering time, respectively, suggesting that JA signals are converted into tissue- and stage-specific outputs by specific TF-JAZ complexes. Expression of the JA-Ile receptor COI1 in discrete flower parts is also tightly regulated, strengthening the notion of the importance of tissue and stage specificity in JA-mediated responses (Jewell and Browse, 2016).

Here we present an example of systemic regulation where, by recruiting photoperiodic and JA signaling, plants can coordinate two processes: floral initiation and senescence. This example of regulatory plasticity can help us understand how plants have evolved to respond to external stimuli and may be used to design new strategies to improve fitness in a changing environment.

RESULTS

CO presence in flowers and genetic analyses suggest a role of CO in flower senescence and abscission

Changes in *CO* expression have a strong effect on the floral transition (Samach et al., 2000), and the phenotypes associated with its overexpression and suppression are early and late flowering, respectively (Simon et al., 1996; Table 1). Surprisingly, plants with altered accumulation of *CO* also showed clear differences in flower phenology; plants overexpressing CO under the 35S promoter, namely 35S:*CO*, 35S:*CO*:CTAPi, and 35S:*CO*:GR (*co-2*) treated with the steroid dexamethasone (Simon et al., 1996), exhibited accelerated flower senescence and abscission compared with wild-type Columbia-0 (Col-0), whereas the transfer DNA-null mutant plants, *co-10* and untreated 35S:*CO*:GR (*co-2*), had a significant delay ($p < 0.001$) in both parameters (Figure 1A; Table 1; Supplemental Figure 1A and 1B). The first flower showing senescence and abscission symptoms according to Bleecker and Patterson, 1997 under long-day (LD, 16 h light/8 h night) conditions was the flower at positions 5 and 6, respectively (detailed in Supplemental Figure 2A and 2B), both, in Col-0 and L*er* wild types (WTs).. In contrast, *CO*-overexpressing flowers showed accelerated responses, with senescence and abscission symptoms observed at positions 2–3 in 35S:*CO* and 35S:*CO*:CTAPi and 1–2 in dexamethasone-treated 35S:*CO*:GR (*co-2*), whereas *co-10* and untreated 35S:*CO*:GR (*co-2*) flowers exhibited delayed responses, with symptoms observed at positions 8–10 and 9–11, respectively (Figure 1A; Table 1; Supplemental Figure 2A and 2B). To confirm these phenotypes at the molecular level, the expression of the senescence marker genes *SAG13* and *SAG29* (*AtSWEET15*) in flowers was analyzed (Yin et al., 2015; Dhar et al., 2020). 35S:*CO* plants showed an induction in mRNA levels, whereas *co-10* showed a clear reduction in *SAG* gene expression (Figure 1B). We also monitored senescence in

Plant(condition)	Flowering time[a]		Senescence[b]	Abscission[c]
	Rosette	Cauline		
Col-0 (long days)	14.0 ± 1.3	3.9 ± 0.4	5.1 ± 0.9	6.6 ± 1.3
35S:*CO*	4.5 ± 0.8	1.5 ± 0.5	1.8 ± 0.6	2.8 ± 0.6
co-10	45.2 ± 2.6	8.5 ± 1.5	8.4 ± 1.2	9.7 ± 1.0
35S:*CO*:CTAPi	7.3 ± 0.6	2.3 ± 0.4	2.2 ± 0.8	3.2 ± 0.7
L*er*-0	7.8 ± 0.9	2.4 ± 0.5	4.9 ± 0.8	5.9 ± 0.9
35S:*CO*:GR (*co*-2) +DEX[d]	7.4 ± 0.5	1.6 ± 05	1.2 ± 04	1.6 ± 0.5
35S:*CO*:GR (*co*-2) -DEX[d]	15.3 ± 1.1	4.8 ± 1.1	9.3 ± 1.0	11.0 ± 1.0
Col-0 (short days)	57.5 ± 3.5	12.1 ± 1.8	8.6 ± 1.1	9.6 ± 1.1
Col-0 (RL)	34.2 ± 3.6	9.0 ± 1.8	8.2 ± 1.2	8.9 ± 1.2
Col-0 (BL)	5.6 ± 0.6	2.5 ± 0.6	3.0 ± 0.7	3.9 ± 0.8
35S:*FT*	2.7 ± 0.8	2.0 ± 0.6	4.4 ± 0.5	5.3 ± 0.4
Ft-10	36.2 ± 2.3	8.8 ± 1.5	5.6 ± 1.0	6.6 ± 1.0
aos1-1	13.0 ± 1.1	4.3 ± 0.7	15.0 ± 1.9	16.0 ± 1.9
aos*1-1* 35S:*CO*	5.5 ± 0.5	1.5 ± 0.5	5.1 ± 1.0	6.3 ± 1.0
aos1-1 co-10	43.2 ± 3.4	8.8 ± 1.8	19.6 ± 1.5	21.0 ± 1.1
coi 1-1	14.9 ± 1.9	3.7 ± 0.6	14.4 ± 2.0	16.0 ± 2.3
coi 1-1 35S:*CO*	5.4 ± 0.6	1.4 ± 0.5	2.8 ± 1.1	3.8 ± 1.1
co-10 p*CO-CO*	13.9 ± 1.0	3.6 ± 0.8	6.2 ± 0.6	7.8 ± 0.6
co-10 pCO-CO$^{1281A+K282A}$#2	16.3 ± 2.4	3.3 ± 0.7	8.6 ± 0.8	10.8 ± 0.9
co-10 pCO-CO$^{1281A+K282A}$#11	14.2 ± 2.3	3.6 ± 1.2	8.1 ± 0.8	10.8 ± 1.1

Table 1. Flowering time, senescence, and abscission from the different genotypes, mutants, and crosses used in this study.
Data are the mean ± SD of at least 50 plants.
* Plants at 10 days after germination were treated with dexamethasone (DEX) (10 μM) once per week until end of experiment.
[a]Number of rosette (excluding cotyledons) and cauline leaves.
[b]Flower positions of the first flower showing senescence symptoms.
[c]Flower positions of the first flower showing abscission symptoms.
[d]Plants at 10 days after germination were treated with dexamethasone (10 μM) once per week until the end of the experiment.

different light regimens (Table 1; Supplemental Figure 1C and 1D) that promote natural destabilization of the CO protein, affecting *Arabidopsis* flowering time (Table 1). In short days (8 h light/16 h dark), *CO* mRNA levels are lower during daytime compared with those under LDs (Austen et al., 2017), whereas growth under LDs in chambers supplemented with lights of different monochromatic wavelengths promotes changes in the stabilization of the protein mediated by different photoreceptors (Valverde et al., 2004). Under blue light (BL)-enriched conditions, cryptochromes and PhytochromeA stabilize CO (Valverde et al., 2004; Liu et al., 2008), whereas growth under red light (RL)-enriched conditions promotes CO degradation through a PhytochromeB-mediated signal (Valverde et al., 2004; Lazaro et al., 2015). Plants senesced earlier under LDs than short days, and although BL promoted early senescence and abscission, RL delayed them (Table 1; Supplemental Figure 1C and 1D). These results strongly suggested a role of CO in control of flower senescence and abscission. Because the main target of CO in the floral transition is the florigen gene *FT* (Samach et al., 2000), we also analyzed flower senescence and abscission in *FT*-overexpressing and -knockout mutant plants (Table 1; Supplemental Figure 1B). However, in contrast to the *co-10* mutant and CO overexpressor, the *ft-10* mutant and 35S:*FT* plants showed no significant differences in flower senescence and abscission compared with the WT, suggesting that CO regulation of these traits is independent of *FT*.

This previously unnoticed phenotype suggested a different function for CO in *Arabidopsis* flowers than canonical floral induction in leaves and prompted us to analyze *CO* expression and protein accumulation in floral organs. First, expression of *CO* was monitored in Col-0 plants transformed with a fusion of the 2-kb *CO* promoter with the *mGFP6* reporter gene by measuring GFP fluorescence in 10-day-old seedlings and mature flowers using a fluorimeter (Supplemental Figure 3A). *CO* promoter activity was visible in seedlings and even more so in flowers. Then we examined the promoter activity of *CO* in floral organs, namely sepals, petals, stamens, and carpels, by confocal microscopy (Figure 1C). The promoter activity of *CO* seemed to be higher in all floral organs than in leaf organs and was not restricted to vascular cells as in leaves (An et al., 2004) but was widely distributed in diverse floral organ cells (Supplemental Figure 3B). *pCO:mGFP6* fluorescence and *CO* mRNA levels in petals were higher at stage 12 than at the more mature stages 14 and 16 (Supplemental Figure 3C and S3D). The broad distribution of fluorescence in mature floral whorls also suggested a role of CO in flowers other than its canonical role in flower initiation.

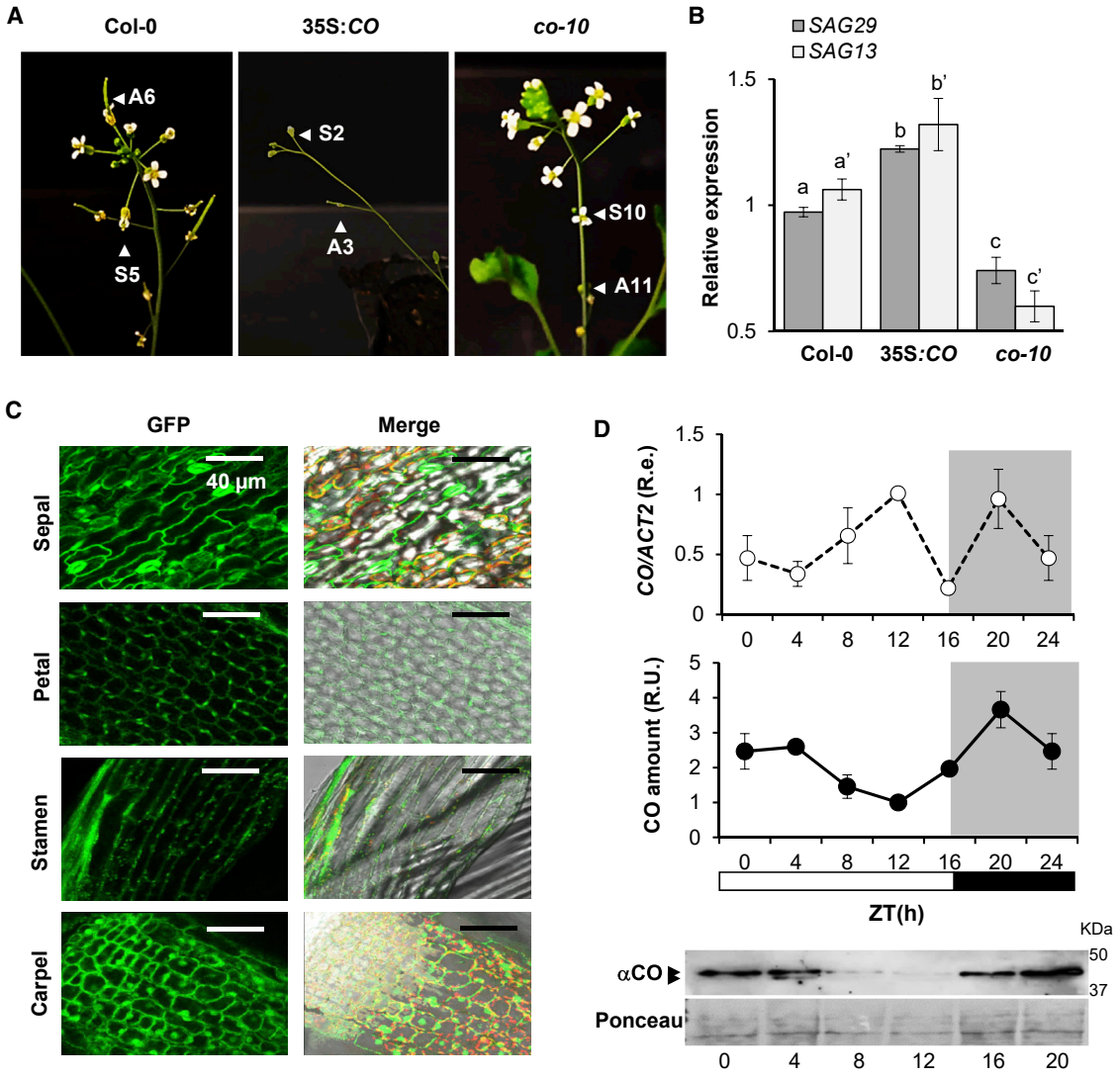

Figure 1. CO promotes flower senescence and abscission.

(A) Flower senescence and abscission phenotypes of WT, 35S:*CO*, and *co-10* plants. Flower positions for senescence (S) and Abscission (A) phenotypes are marked by white arrows.

(B) qRT–PCR analyses of *SAG13* (light gray) and *SAG29* (dark gray) in WT, 35S:*CO*, and *co-10* flowers at stage 14 (plants grown under LDs and sampled at ZT16). *ACT2* was used as a control. Error bars indicate standard deviation (SD) from three independent experiments. $P < 0.05$, one-way ANOVA and Tukey's test.

(C) Confocal images of epidermal cells in floral organs (sepal, petal, stamen, carpel) of p*CO*:*mGFP6* plants. Left panels: GFP fluorescence. Right panels: merged fluorescence and bright field image. Scale bars represent 40 μm.

(D) Time-course qRT–PCR analysis of *CO* expression (top panel) in WT petals (stage 14, LD). *ACT2* was used as a control. R.e., relative expression. Error bars, SD from three independent experiments. Bottom panel: 24-h CO protein accumulation analysis in WT petals (stage 14, LD) and quantification of protein levels in three immunoblot replicates (±SD) using αCO. Ponceau staining was used as a control. Arrowheads point to the CO double band.

We then determined *CO* mRNA and protein levels in WT whole flowers (Supplemental Figure 4A), confirming the presence of *CO* transcript and protein in flowers of Col-0. Predictably, *CO* transcript and protein levels were higher in flowers of 35S:*CO* plants than in WT flowers and absent in flowers of *co-10* mutants (Supplemental Figure 4B). To further characterize the specific expression of *CO* in petals we analyzed *CO* expression in WT petals over a 24-h cycle (Figure 1D, top panel). In LD *CO* mRNA followed a diurnal expression pattern with peaks at Zeirgeber Time (ZT) 12 and ZT20, differing from the leaf expression pattern, in which the highest expression was observed in the evening at ZT16 (Supplemental Figure 4C). During an LD cycle, the CO protein in petals peaked at ZT20 into the night (Figure 1D, bottom panel), again differing from the CO pattern in leaves where CO protein peaks at ZT12–ZT16 (Valverde et al., 2004; Andrés and Coupland, 2012). However, in plants growing in different light regimens, *CO* was equally expressed in petals (Supplemental Figure 4D), whereas the protein levels showed a similar pattern as described in leaves (Valverde et al., 2004; Supplemental Figure 4E), suggesting that photoreceptors

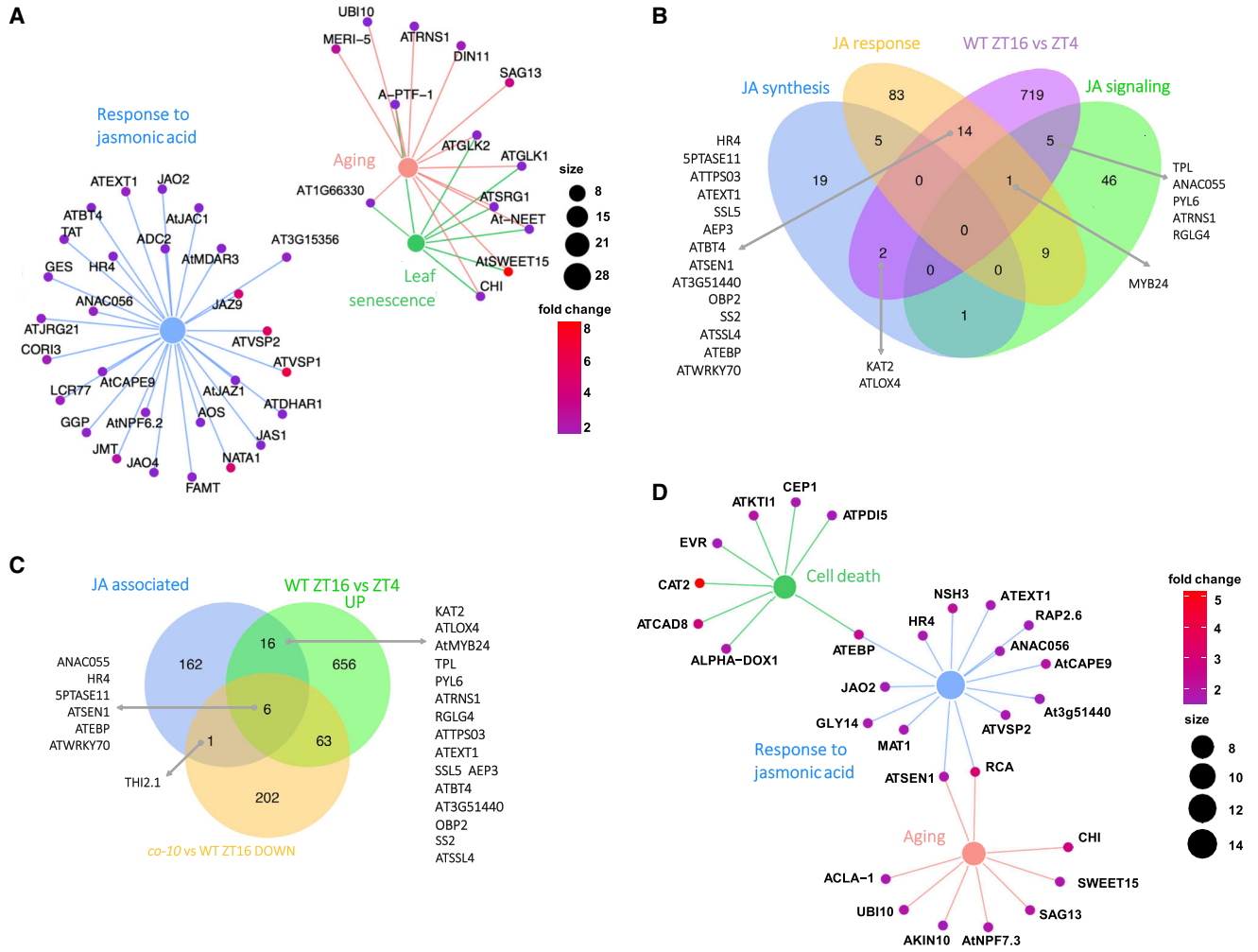

Figure 2. *CO* participates in regulating the expression of JA-associated genes.

(A) GO enrichment analysis for upregulated genes identified in the comparison of 10-day-old 35S:*CO* versus WT seedlings (LD, ZT16). The diagram shows GO terms of interest and associated differentially expressed genes with corresponding fold changes.

(B) Venn diagram showing JA-associated genes upregulated in WT petals (stage 14, LD) at ZT16 versus ZT4. Full names and description of abbreviations for gene annotations are included in Supplemental Data 1.

(C) Venn diagram showing JA-associated upregulated genes in WT petals (stage 14, LD) at ZT16 versus ZT4 overlapping with JA-associated genes downregulated in the *co-10* versus WT (petals, ZT16) pairwise comparison. Full names and description of abbreviations for gene annotations are included in Supplemental Data 1.

(D) Gene Ontology (GO) enrichment analysis for upregulated genes in the 35S:*CO* versus WT pairwise comparison in petals (stage 14, LD, ZT4). The diagram shows GO terms of interest and associated differentially expressed genes with corresponding fold changes.

are also involved in CO stability in floral organs. The differences in *CO* expression and protein turnover in leaves and flowers also hinted at a different mechanism for regulation of CO in flowers.

CO participates in the control of flower senescence and abscission mediated by JA

To further characterize the role of CO in the senescence and abscission responses shown in the previous section, we analyzed data from a transcriptomics study comparing WT and *CO*-overexpressing whole seedlings under LD conditions at ZT16. The analysis revealed a significant effect of *CO* overexpression on the aging process and senescence (Figure 2A and Supplemental Figure 5A–5C). Expression of many *SAG* genes (*SAG13*, *ATBCB*, and *ATSWEET15*) showed pronounced upregulation in 35S:*CO* plants compared with WT plants (Supplemental Figure 5C). Remarkably, a significant number of JA-associated genes (25 of 201; Supplemental Data 1), including JA synthesis, signaling, and response genes, were also upregulated in 35S:*CO* plants (Figure 2A and Supplemental Figure 5A; Supplemental Table 1). Because JA is a phytohormone that is emerging as a key player in control of senescence (Jibran et al., 2013; Fang et al., 2016), the results suggested a possible age-related senescence association between *CO* overexpression and the JA pathway.

This hypothesis was reinforced by a transcriptomic analysis comparing RNA sequencing (RNA-seq) data from petals collected at ZT4 and ZT16 from WT, *co-10*, and 35S:*CO* plants; these time points were chosen because it has been demonstrated that CO activity is different in the morning than in the evening (Valverde et al., 2004; Supplemental Data 2). Genes

upregulated in the WT at ZT16 were compared with those at ZT4 by Gene Ontology (GO) enrichment analysis; the JA pathway was significantly enriched. Several JA marker genes were significantly upregulated at ZT16 compared with ZT4, indicating that the JA signal in petals is preferentially activated in the evening (Figure 2B and Supplemental Figure 6A). In *co-10* mutants, 6 of 22 JA-associated genes were downregulated, particularly at ZT16 (Figure 2C), and according to GO enrichment analysis, the JA pathway was not significantly induced, indicating that CO was important to trigger the JA pathway (Supplemental Figure 6B and 6C). Of the 22 JA-associated genes activated at ZT16, only those related to the JA response were significantly repressed in *co-10* plants, suggesting that CO is probably involved in activating the late responses mediated by the JA pathway rather than early responses, such as biosynthetic processes. Petals of 35S:*CO* flowers showed high expression of JA-associated genes, particularly at ZT4 (Figure 2D), indicating an enrichment of JA pathway genes when *CO* was overexpressed. Genes activated by CO in petals significantly differed from those activated in seedlings, hinting at a different role of CO in these two tissues (Supplemental Figure 7A). In petals, marked differential expression was observed in Col-0 compared with seedlings. In this sense, although expression of JA response genes in petals was significantly altered in WT and *co-10* samples, CO leaf target genes (such as *FT* and *SOC1*) showed no significant differences in expression at ZT4 or ZT16 in petals in contrast to other genes involved in the photoperiodic response, such as *CDF3* or *CDF5* (Supplemental Data 2; Supplemental Figure 7B). The accuracy of the RNA-seq data was confirmed by selection of a set of random genes and quantification by qRT–PCR using cDNA from the same RNA samples. The Pearson correlation coefficients between qRT–PCR and RNA-seq data were 0.9718367, 0.9544037, 0.8568816, 0.9424255, and 0.9574517 for *TOC1*, *HY5*, *PRR7*, *LEA3*. and *CCA1*, respectively, indicating a good correlation between experimental approaches (Supplemental Figure 8). Overall, our transcriptomic analysis suggests that CO may promote accelerated senescence through transcriptional regulation of JA response genes.

We also crossed the *CO* mutant and overexpression line with plants carrying mutations in genes involved in JA synthesis (*allene oxide synthase 1* [*aos1-1*]; Park et al., 2002) and signaling (*coronatine insensitive 1* [*coi1-1*]; Xie et al., 1998) and analyzed the effect on flower senescence and flowering time (Table 1; Figure 3 and Supplemental Figures 2–9). AOS1 is one of the first enzymes involved in JA synthesis, and COI1 is an essential component of the receptor complex involved in almost all JA-dependent responses (Chini et al., 2007; Thines et al., 2007). *Aos1-1* 35S:*CO* and *coi1-1* 35S:*CO* plants showed no significant difference in flowering time compared with 35S:*CO* plants (Table 1; Supplemental Figure 9A and 9B), although the *coi1-1* mutant has been reported to show a small acceleration of flowering time compared with WT plants under LDs (Robson et al., 2010; Zhai et al., 2015). Although this may be caused by *CO* ectopic expression, a small effect on flowering time was observed in the double mutant *aos1-1 co-10* compared with *co-10* plants, supporting the specific effect of CO on the process (Supplemental Figure 9C). Phenotype analysis of flowers of *aos1-1* 35S:*CO* and *coi1-1* 35S:*CO* compared with the single mutants showed that the delayed floral senescence and abscission characteristics of the *aos1-1* and *coi1-1* mutants were strongly suppressed by *CO* overexpression. In contrast, floral senescence and abscission were enhanced in *aos1-1 co-10*, supporting the hypothesis that *CO* affects JA-mediated flower senescence downstream of AOS1 and COI1 (Figure 3A–3D and Supplemental Figures 2 and 9D). Accordingly, 35S:*CO*, *aos1-1* 35S:*CO*, and *coi1-1* 35S:*CO* plants showed *SAG13* and *SAG29* transcript levels that were significantly higher than those of the single mutants *aos1-1* and *coi1-1* (Figure 3E and 3F).

CO interacts with JAZ3 through its ZIM-like domain and inhibits its activity

Because we found no significant differences in JA levels between 35S:*CO* and *co-10* flowers, even though they show differences in transcriptional expression of JA-associated genes, we decided to explore whether CO can regulate the JA response in flowers at the protein level. CO can directly interact with proteins involved in JA signaling (such as JAZ proteins), some of which (such as JAZ3) are conspicuously expressed in petals (Supplemental Figure 10A), as well as COI1 and MYC2. The CO protein has three distinct domains (Figure 4C): two amino-terminal b-boxes, the middle part, and the C-terminal domain (CCT-CONSTANS, CO-like, and TOC1) (Tiwari et al., 2010; Valverde, 2011). To identify the domain of CO putatively mediating the interaction with JA signaling components, we cloned the three domains of CO in the bait vector pJG4-5 and the complete open reading frames of interactors in the prey vector pEG202 to perform yeast two-hybrid (Y2H) assays. The Y2H assays showed that JAZ3 interacted with the middle part of CO, whereas COI1 and MYC2 showed no interaction (Figure 4A and Supplemental Figure 10B). Similar tests with added coronatine, a bacterial toxin that mimics JA-Ile (Howe et al., 2018), and a direct ligand of COI1 that promotes JAZ-COI1 interaction also produced negative results (Supplemental Figure 10B).

Next we performed transient bimolecular fluorescence complementation (BiFC) assays of the Yellow Fluorescenct Protein (YFP) in *Nicotiana benthamiana*, in which we cotransformed the N-terminal part of YFP (YFN) fused to the complete CO protein and the C-terminal part of YFP (YFC) fused to JA signaling-related proteins and controls (Figure 4B and Supplemental Figure 11A and 11B). A strong YFP nuclear signal was observed under confocal microscopy in cells expressing CO with JAZ3 (Figure 4B, top panel) but also with JAZ1 and JAZ5 and, at a weaker intensity, with JAZ6 and JAZ12 (Supplemental Figure 11A), roughly coinciding with expression of these genes in petals (Supplemental Figure 10A) and suggesting specificity in CO-JAZ interaction. Unexpectedly, in this assay, we detected CO binding to COI1 (Figure 4B, bottom panel), whereas MYC2 and many other JAZ proteins did not show interaction with CO (Supplemental Figure 11A). These results confirmed the CO-JAZ interaction and also suggested that the CO-COI1 interaction detected by BiFC may be indirect, possibly mediated by other partners, likely endogenous *Nicotiana* JAZs, present in the plant and absent in yeast.

To verify whether the effect of CO on JA-responsive genes is due to the physical interaction between CO and JAZs and not to transcriptional regulation, we performed chromatin immunoprecipitation (ChIP)–qPCR experiments using CO-specific antibodies

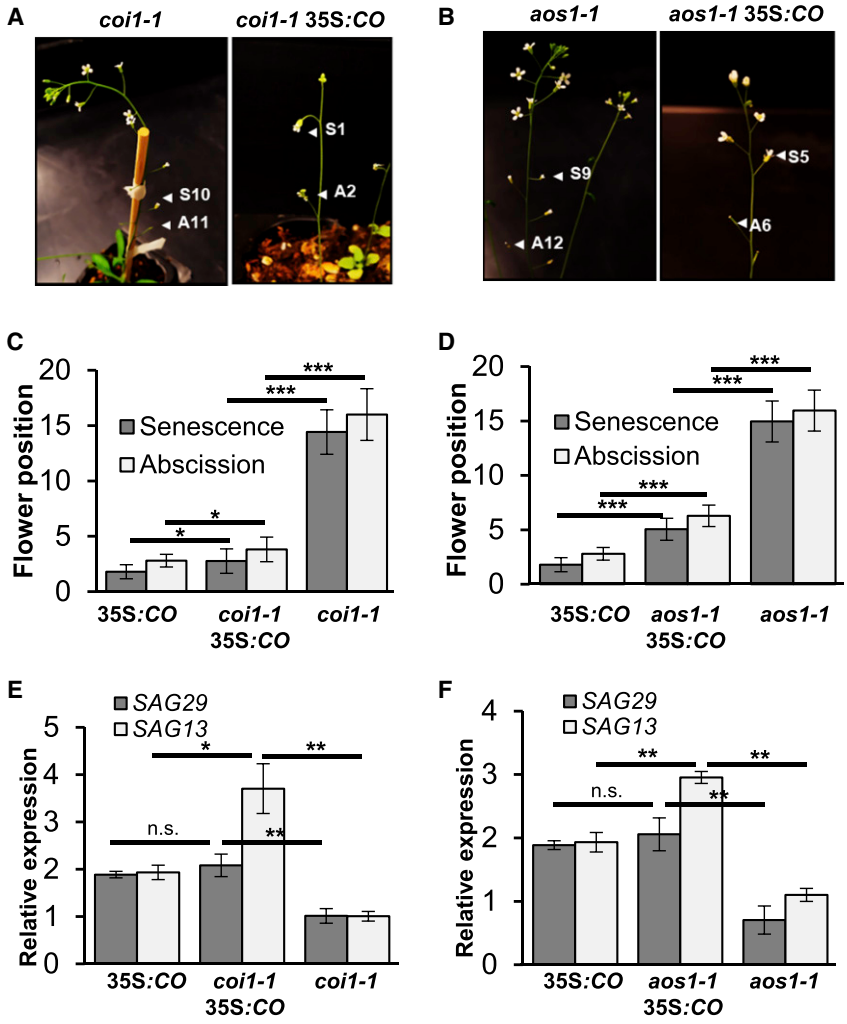

Figure 3. Genetic interaction between the 35S:*CO* line and JA pathway mutants *coi1-1* and *aos1-1*.

(A and B) Flower senescence and abscission phenotypes of *coi1-1* and *coi1-1* 35S:*CO* plants and *aos1-1* and *aos1-1* 35S:*CO* plants as in Figure 1A.

(C and D) Position of flowers showing yellowing (dark gray) and A (light gray) in 35S:*CO*, *coi1-1* 35S:*CO*, and *coi1-1* plants © and in 35S:*CO*, *aos1-1* 35S:*CO*, and *aos1-1* plants **(D)**. Error bars, SD of more than 50 inflorescences.

(E and F) qRT–PCR analyses of *SAG13* (light gray) and *SAG29* (dark gray) in 35S:*CO*, *coi1-1* 35S:*CO*, and *coi1-1* flowers © and in 35S:*CO*, *aos1-1* 35S:*CO*, and *aos1-1* flowers **(F)** at stage 14 (plants grown under LD and sampled at ZT16). *ACT2* was used as a control. Error bars, SD from three independent experiments.

in 35S:*CO* and *co-10* seedlings. First, we analyzed the *FT* promoter as a control target gene, observing significantly higher enrichment of the CORE1/2 site (Tiwari et al., 2010) when comparing 35S:*CO* plants with *co-10* mutants (control). However, the analyzed amplicons in other JA-responsive gene (*JAZ1*, *JAZ3*) promoters did not show significant differential enrichment (Supplemental Figure 12). These results demonstrate that JA-responsive genes are not direct targets of CO.

Based on the positive interation between CO-JAZ, we compared the domain structures of both protein families. We found that BBX proteins similar to CO (CO-like), ZIM proteins, and JAZ proteins belong to a superfamily of plant GATA-like TFs (Manfield et al., 2007) and share several structural features (Supplemental Figure 13). Some ZIM proteins contain the characteristic ZIM domain and an internal CCT similar to the CO terminal CCT. JAZ proteins contain a highly conserved region, the TIFY motif (TIFF/YXG), within the ZIM domain that mediates homo- and heteromeric interactions between most JAZs (as well as the interaction with the NOVEL INTERACTOR OF JAZ adaptor protein) (Chini et al., 2009; Chung and Howe, 2009). After performing sequence homology analysis, we found that the middle part of CO, which mediates the interaction with JAZ3, has characteristics of a ZIM-like domain (ZIM*), including a TIFY-like motif (NIKY in the CO sequence, amino acids 235–238) (Figure 4C). To test the function of the CO ZIM* domain in the interaction with JAZ3, we mutated the middle part of CO, disrupting the NIKY motif ZIM* $^{(I236A+K237A)}$ (middle*; Figure 4C). Y2H assays showed that modification of the CO NIKY motif disrupted the interaction between the middle part of CO and JAZ3 (Figure 4C, bottom panel), suggesting an undescribed critical role of the intermediate ZIM-like domain of CO in the CO-JAZ3 interaction.

Next, we explored the physiological role of the CO-JAZ3 interaction in *Arabidopsis*. We transformed *co-10* mutant plants with a construct containing the *CO* promoter fused to a mutated form of *CO* (p*CO-CO**$^{(I236A+K237A)}$), including the same modifications in the NIKY motif assayed previously in the Y2H assay. A *co-10* plant transformed with the same WT construct (p*CO-CO*) was used as a control. As shown in Figure 4D and 4E, flower senescence and abscission were delayed in *co-10* p*CO-CO**$^{(I236A+K237A)}$ transgenic lines (2 and 11) to an extent similar to that in the *co-10* mutant parent (Figure 1A). In contrast, control *co-10* p*CO-CO* plants showed senescence and abscission similar to those of the WT plants. tThe delay in flower senescence and abscission of *co-10* p*CO-CO**$^{(I236A+K237A)}$ transgenic lines (Table 1) was accompanied by a reduction in the mRNA levels of *SAG13* and *SAG29* compared with *co-10* p*CO-CO* control plants (Figure 4F). These data suggest that the CO-JAZ3 interaction is a limiting factor in the CO-mediated flower senescence and abscission response. However, the flowering time of *co-10* p*CO-CO** transgenic lines was similar to that of Col-0 and *co-10* p*CO-CO* plants and significantly different from that of *co-10* mutants (Table 1; Figure 4G and Supplemental Figure 14), suggesting that the mutation does not affect the flowering function of CO. Therefore, the CO NIKY motif is important for CO-mediated regulation of JA responses in flowers but not CO-dependent regulation of

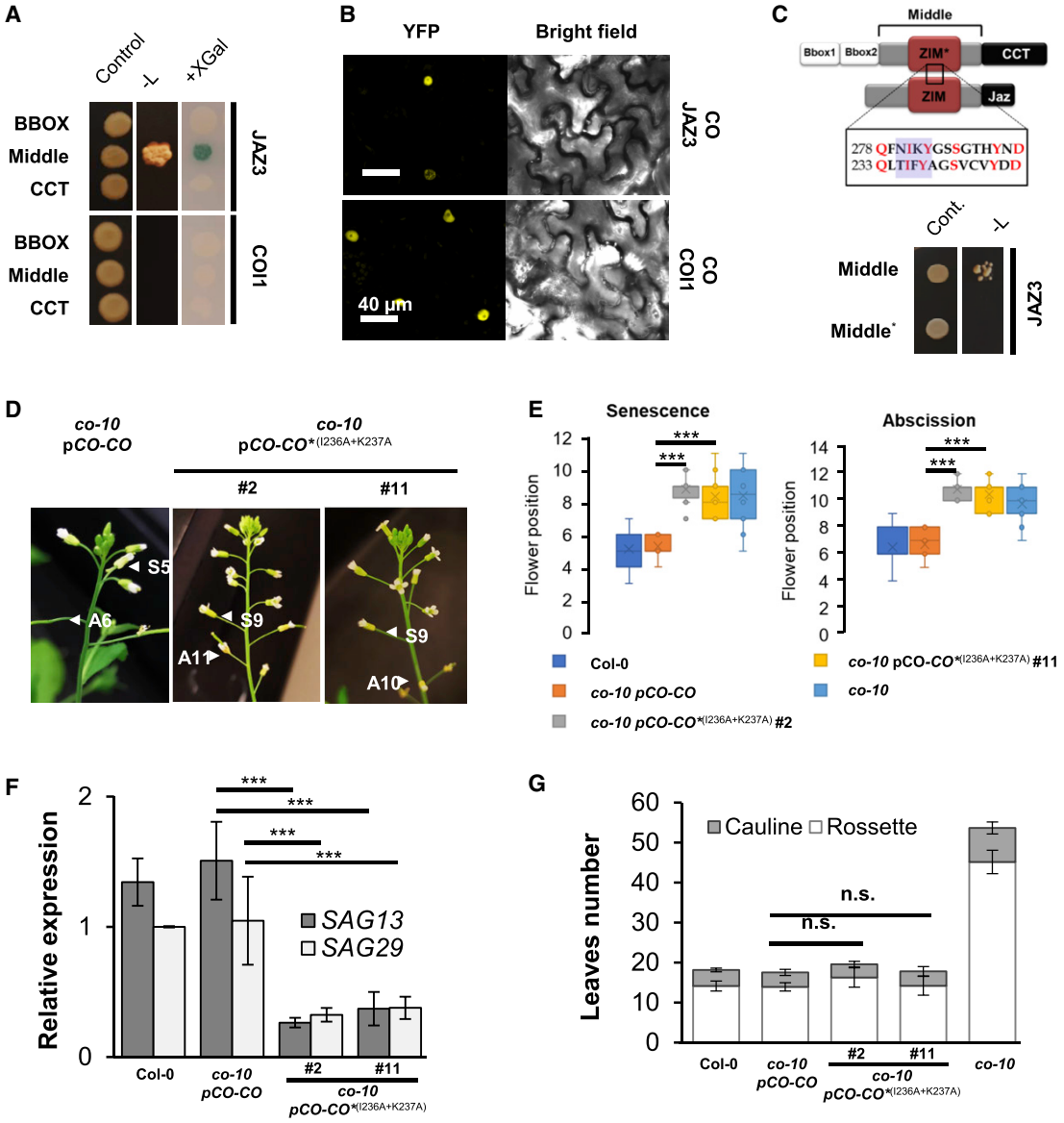

Figure 4. A TIFY-like motif mediates the interaction between CO and JAZ3.

(A) Y2H assays showing the interaction between different parts of CO (BBOX, middle, and CCT), COI1, and JAZ3. Shown are 3-day-old colonies grown in different selective media.

(B) BiFC assays showing the interaction between YFC:CO and YFN:JAZ3 (top panels) and YFC:CO and YFN:COI1 (bottom panels) in *Nicotiana* leaf epidermal cells. Positive and negative controls are shown in Supplemental Figure 11. Left panels: reconstituted YFP fluorescence. Right panels: bright-field images. Scale bars represent 40 μm.

(C) Top: cartoon showing the conserved JAZ-interacting motifs in CO (top, NIKY) and JAZ3 (bottom, TIFY). Bottom: Y2H assay showing the lack of interaction between JAZ3 and the middle domain of CO mutated in the NIKY motif (Middle$^{*(I236A+K237A)}$). Images show 3-day-old colonies.

(D) Flower S and A phenotypes of the WT, *co-10* p*CO*:*CO*, and two independent *co-10* plant lines expressing p*CO-CO*$^{*(I236A+K237A)}$. Position of flowers is as in Figure 1©.

(E) Position of flowers showing yellowing (left) and A (right) in WT, *co-10* p*CO*:*CO*, and two independent *co-10* plant lines expressing p*CO-CO*$^{*(I236A+K237A)}$. Error bars, SD of more than 50 inflorescences.

(F) qRT–PCR analyses of *SAG13* (dark gray) and *SAG29* (light gray) in flowers (stage 14) of WT, *co-10* p*CO*:*CO*, and two independent *co-10* plant lines expressing p*CO-CO* $^{*(I236A+K237A)}$ (plants grown under LD and sampled at ZT16). *ACT2* was used as a control. Error bars, SD from three independent experiments.

(G) Comparison of flowering time in the WT, *co-10*, *co-10 pCO:CO*, and two independent *co-10* lines expressing *pCO-CO*$^{*(I236A+K237A)}$ (bottom). Flowering time measurement: light gray bars, rosette leaves; dark gray bars, cauline leaves. Error bars, SD of more than 50 plants.

flowering time, revealing an uncharacterized dual role of CO in regulating flower development.

COI1 targets both CO andJAZ3 for degradation

We then investigated the relationship between CO and JAZ3 and determined whether the interaction of CO with JAZ3 (and other JAZ proteins) could affect CO activity. Because of the high functional redundancy of JAZ proteins (Chini et al., 2016), we used the *aos1-1* and *coi1-1* mutants, which are severely affected in JA signaling. Although *CO* expression was roughly similar in *aos1-1* 35S:*CO* and *coi1-1* 35S:*CO* plants compared with 35S:*CO* lines (Supplemental Figure 15A and 15B) at the protein level, the two lines displayed a significantly higher amount of CO protein than 35S:*CO* plants (Figure 5A and 5B). CO levels were also higher in *coi1-1* and *aos1-1* single mutants than in Col-0 plants, and this was particularly evident in the *coi1-1* mutant, which had CO levels similar to those of the *cop1-4* mutant (Supplemental Figure 15C and 15D). These results showed that the lack of synthesis or signaling of JA stabilized CO protein levels in the petals. Because COI1, as well as COP1, is an E3-ubiquin ligase, these results also suggested that CO may be a target for degradation by COI1 (Thines et al., 2007).

To test the possible interaction of COI1 with the JAZ3-CO complex detected by BiFC, we first confirmed the interaction between YFN:COI1 and YFC:JAZ3 and reconstitution of YFP (Supplemental Figure 11A) and then performed a co-immunoprecipitation (coIP) assay using *N. benthamiana* leaves transiently expressing *CO*, *YFN:COI1*, and *YFC:JAZ3*. Following IP with GFP-trap, which recognizes reconstituted YFP, we detected CO protein in the lysates of these leaves using αCO and αGFP (Figure 5C). These results show that CO, JAZ3, and COI1 can form a complex. For further confirmation, we performed an *in vivo* fluorescence resonance energy transfer (FRET) assay using *Nicotiana* expressing CO fused to CYAN FLUORESCENT PROTEIN (*CO:CFP*), *YFN:COI1*, and *YFC:JAZ3*. Only when *CO:CFP* was coexpressed with *YFN:COI1 and YFC:JAZ3, which* reconstituted the YFP signal, was the FRET signal detected, confirming the triple interaction (Figure 5D, top panel). To quantify the interaction, the obtained results were normalized using the normalized FRET (N_{FRET}) method (Xia and Liu, 2001; Figure 5D, bottom graphic), and the significant differences compared with the controls strongly supported the direct *in vivo* interaction between CO, JAZ3, and COI1.

Identification of the CO-JAZ3-COI1 complex and the increased CO stability in *coi1-1* mutant protein extracts led us to investigate degradation of CO by COI1. We performed sequential immunoblot measurements of CO protein levels in lysates of *Nicotiana* leaves expressing a hemagglutinin (HA):CO fusion incubated for 30 min with lysates from COI1- and JAZ3-overexpressing plants (Figure 5E and Supplemental Figure 16A). A decrease in HA:CO protein levels was observed when the HA:CO lysate was incubated with the lysate from COI1-expressing leaves, but this effect was dramatically enhanced when HA:CO lysate was incubated with a mixture of lysates from COI1- and JAZ3-expressing leaves (Supplemental Figure 16A). A similar experiment with the recombinant *Arabidopsis* TF FLOWERING LOCUS M (FLM) and the native *Nicotiana* protein GLYCERALDEHYDE-3-PHOSPHATE DESHYDROGENASE (GAPDHC) showed no significant degradation (Supplemental Figure 16A and 16B). Although *CO* transcript levels in flowers of *co-10* p*CO-CO*$^{*(I236A+K237A)}$ transgenic lines were not significantly different from those in Col-0 and *co-10* p*CO-CO* plants (Supplemental Figure 16C), protein levels were significantly higher (Figure 5F and Supplemental Figure 16D), suggesting that the lack of interaction between JAZs and CO promoted CO accumulation *in vivo*. Because *Nicotiana* extracts may have natural sources of JAs, we decided to test whether external treatment with Methil jasmonate affected the degradation of CO and JAZ3. Treatment of *Nicotiana* extracts accumulating HA:CO, YFC:JAZ3, and YFN:COI1 with Methil jasmonate significantly enhanced the degradation of CO and JAZ3 (Figure 5G; Supplemental Figure 16F and 16G). Therefore, our results suggest that JA mediates the formation of a protein complex between CO-JAZ3-COI1 that promotes CO and JAZ3 degradation.

DISCUSSION

In this work, we describe a previously unidentified function of the main photoperiodic regulator CO in flower senescence and abscission. In previous studies, *CO* was identified as being differentially expressed in the shoot apical meristem during the early stages of floral differentiation, and although *CO* was upregulated, *FT*, its main target, was not (Wellmer et al., 2006; Chen et al., 2018). This hinted to a possible different role of CO compared with that described in induction of flowering by photoperiod (Suárez-López et al., 2001; Serrano-Bueno et al., 2021). Here we describe the presence of CO protein in floral organs with a novel pattern of expression and a role in flower senescence. Under natural conditions where CO abundance is reduced, such as in the *CO* mutants or under short day or RL conditions, flower senescence decreases, whereas under conditions in which CO protein is more abundant, such as under LD or BL conditions or in *CO*-overexpressing plants, flower senescence is enhanced (Figure 1; Table 1; Supplemental Figure 1). The implication of different light and CO functions in the flower raises interesting questions regarding the long-known delay of senescence by RL (Sakuraba, 2021) and may explain why RL has been used to augment longevity in roses and other ornamental flowers in traditional horticulture and cut flower markets (Heo et al., 2004). Identification of senescent and abscission responses in the flowers of *co* mutant plants also indicated a different role of CO in flowers other than the canonical floral transition function in the leaves. To avoid out-of-season flowering, CO activity is modulated by complex translational and post-translational regulation mechanisms (Valverde et al., 2004; Andrés and Coupland, 2012). In flowers, we observed that *CO* mRNA accumulated at a high level in different floral organs and showed a diurnal pattern of expression different from that in the leaves.

Comparison of transcriptomics data between leaves and petals also indicated that *CO* overexpression caused upregulation of genes associated with senescence, aging, and cell death, processes regulated by the hormone jasmonic acid. In WT petals, JA-associated genes are preferentially activated in the evening, as described previously in other organs (Jewell and Browse, 2016). *co* mutation and *CO* overexpression altered this daily expression pattern, with gene expression decreasing in the *co-10* knockout and increasing in CO-overexpressing plants

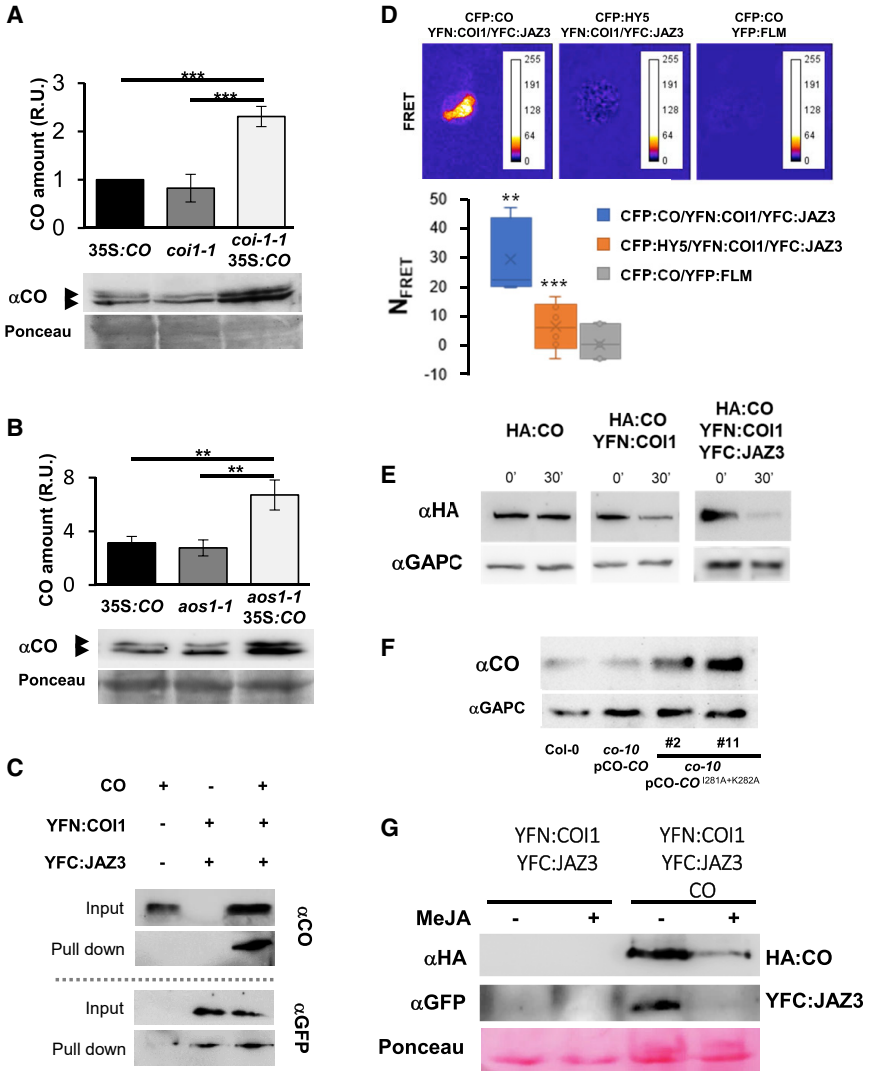

Figure 5. COI1 promotes the degradation of both CO and JAZ3.

(A) αCO immunoblot analysis of CO protein accumulation in 35S:*CO*, *coi1-1*, and *coi1-1* 35S:*CO* flowers, at stage 14 from plants grown under LD. Samples were collected at ZT16, and quantification of protein levels was perfomed in three replicates. Ponceau staining was used as a loading control.

(B) αCO immunoblot analysis of CO protein accumulation in 35S:*CO*, *aos1-1*, and *aos1-1* 35S:*CO* flowers (stage 14, LD, ZT16, and quantification of protein levels in three replicates). Ponceau staining was used as a loading control.

(C) Co-immunoprecipitation of CO, YFN:COI1, and YFC:JAZ3 from *N. benthamiana* leaves using GFP-trap and detection with αCO (top panels) or αGFP (bottom panels).

(D) FRET analysis of CO, COI1, and JAZ3. CO was fused to CFP, and YFP was reconstituted by YFN:COI1/YFC:JAZ3. CFP:HY5 and YFP:FLM were used as negative controls. The proteins were co-expressed in *N. benthamiana* leaves, and normalized FRET (N_{FRET}) was measured in 10 cells.

(E) HA immunoblot analysis of HA:CO accumulation after co-incubation with *N. benthamiana* lysates expressing COI1 and COI1-JAZ3. Ponceau staining and immunodetected GAPDHC (αGAPC) were used as loading controls.

(F) αCO immunoblot analysis of CO accumulation in flowers of WT, *co-10* p*CO:CO*, and two independent *co-10* plant lines expressing p*CO-CO*$^{*(I236A+K237A)}$ grown under LD and collected at ZT16 (bottom panel). Ponceau staining and αGAPC-immunodetected GAPDHC were used as loading controls.

(G) Immunoblots showing HA:CO (αHA) and YFP:JAZ3 (αGFP) degradation with (+) or without (−) MeJA (2 mM) addition. Incubation time was 30 min. Ponceau staining was used as a control.

(Figure 2). The fact that the canonical gene targets of CO, *FT*, and *SOC1* were not altered in the evening or in the *co-10* mutant also suggested that the role of CO in petals was different from that in leaves (Supplemental Data 2; Supplemental Figure 7). *CO* overexpression induced senescence and abscission responses in association with *COI1*, a key JA perception component, and *AOS1*, an essential JA biosynthetic element whose mutant is unable to accumulate the active form of the hormone (Park et al., 2002). Consequently, *co* mutation in the *aos1-1* background delayed senescence, supporting the involvement of CO in JA signaling modulation (Table 1). Surprisingly, *aos1-1* (lack of JA) and *coi1-1* (lack of JA signalling) mutants accumulated high levels of CO protein in the flower, supporting CO stability mediated by COI1 ubiquitin ligase as part of the molecular mechanism involved..

CO is able to interact with JAZ proteins. Although JAZ-DELLA binding has been described and has linked gibberellins with the JA signaling pathway (Hou et al., 2010), this is the first evidence of CO being able to directly interact with these regulatory elements (Figure 4). This interaction is independent of JA and can by itself induce senescence, as suggested by analysis of *CO* overexpression in *coi1-1* and *CO* overexpression in *aos1-1* mutant plants, which suggests a novel mechanism regulating the senescence response (Figure 6). We show that the CO-JAZ3 interaction is due to a structural feature of JAZ repressors and CO, which share a ZIM domain, including a TIFY motif (NIKY in the central part of CO) that promotes JAZ-CO binding. Mutation of the NIKY motif prevented CO-JAZ interactions; the altered motif failed to complement the senescence responses without altering the flowering time of the *CO* knockout plants (Figure 4). The ZIM motif mediates JAZ dimerization (Chini et al., 2009; Chung and Howe, 2009); thus, binding of CO to this motif may effectively sequester JAZ3, keeping it from inhibiting MYC TFs and thereby activating senescence. Finally, the accumulation of ZIM* CO *in vivo*, the results of pull-down and FRET experiments, and the augmented degradation of CO-JAZ3 in the presence of JA (Figure 5) strongly suggest that CO-JAZ3-COI forms a complex that triggers degradation of the CO and JAZ3 proteins.

Our data support a model where, under basal conditions (in the absence of JA), binding of CO to JAZ3, and probably to other JAZs, sequesters the JAZ component and keeps it from

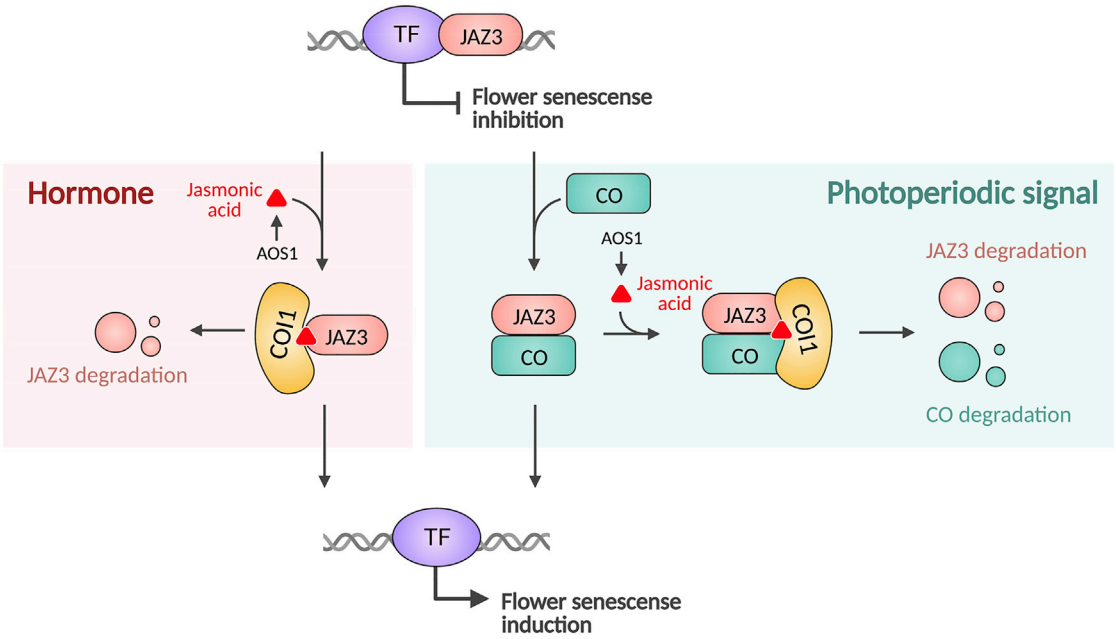

Figure 6. A proposed model illustrating the role of the CO-JAZ3-COI1 interaction in controlling flower S and A in plants.
The current hormone signaling model (left, red background) explains JA activation of S response through the COI1-mediated degradation of JAZ dimers that inhibit TFs (including MYCs) regulating S-related genes. CO (green) can sequester JAZ3 (red), keeping it from repressing TFs (purple) and thereby inducing S. CO-JAZ3 complex is targeted for degradation by COI1, which further activates the S program, acting through the CO (photoperiod) and hormone pathway (green background).

repressing MYCs and/or other TFs (Zhai et al., 2015), promoting senescence. High levels of JA induced JAZ3-CO binding to COI1 and promoted JAZ3-CO degradation, further inducing senescence (Figure 6). Therefore, we propose that, by recruiting CO to a well-established hormonal regulatory pathway, plants can modulate senescence and incorporate temporal/seasonal regulation into the system. This may be a paradigm of how plants can use their plasticity to intertwine different regulatory pathways to control specific tissue and time cues. Understanding these regulatory processes and studying new variants may be important in our race to make plants resilient to global climate change and may also allow us to develop important biotechnological applications in flower longevity and crop production.

METHODS

Plant materials and growth conditions

All *Arabidopsis* strains used in this study are of the Col-0 or L*er* background. *Arabidopsis* mutants *co-10* (Robson et al., 2001), *ft-10* (Yoo et al., 2005), *coi1-1* (Xie et al., 1998), and *aos1-1* (Park et al., 2002) have been described. The plants 35S:*CO*:GR (*co-2*) in the L*er* background and 35S:*CO*:CTAPi (Col-0) were generated by Simon et al. (1996) and Serrano-Bueno et al. (2020), respectively. 35S:*CO*:GR (*co-2*) plants were left untreated, or the steroid dexamethasone was added at 10 days after germination (10 μM) once a week to activate CO nuclear import. The genotypes *coi1-1* 35S:*CO*, *aos1-1 co-10*, *aos1-1* 35S:*CO*, *pCO*(2Kb):*mGFP6*, *pCO*:*CO*, and *pCO*-*CO*$^{*(I236A+K237A)}$ were generated in this study. Plants were grown in controlled cabinets on peat-based compost. Seeds were incubated for 4 days at 4°C in the dark before sowing under LD or short day cycles with temperatures ranging from 22°C (day) to 18°C (night). For light quality experiments, light-emitting diode chambers (CLF floraLEDs, CLF Plant Climatics) were used, with white light (50 μmol m^{-2} s^{-1}) enriched with BL (50 μmol m^{-2} s^{-1}, peak 470 nm) or RL (50 μmol m^{-2} s^{-1}, peak 670 nm) and a half-bandwidth of 20 nm.

Analysis of flower senescence and abscission

Flower senescence and abscission were analyzed in controlled environment cabinets by scoring the positions of the first flower with senescence/abscission symptoms. Flower positions were defined according to the numbering system of Bleecker and Patterson (1997), which identifies flower position 1 as the topmost flower with visible white petals. Data are expressed as the mean of at least 50 individuals ± standard deviation (SD).

Analysis of flowering time

Flowering time was analyzed in controlled environment cabinets by scoring the number of rosette (excluding cotyledons) and cauline leaves. Data are expressed as the mean of at least 50 individuals ± SD.

RNA extraction and qRT–PCR)

One microgram of TRIzol-isolated RNA was used to synthesize cDNA with the Quantitec Reverse Kit (QIAGEN, 205311) following the manufacturer's instructions and diluted to a final concentration of 10 ng μl^{-1}. The primers for qPCR are listed in Supplemental Table 2. qPCRs were performed using an SYBR Fluorescein Kit (Bioline, BIO-96020) on an iQTM5 multicolor real-time PCR detection system (Bio-Rad). The initial concentrations of candidate and reference genes were calculated by means of LingRegPCR software v.11.0 (Ruijter et al., 2009). Normalized data were calculated by dividing the average of at least three

replicates of each sample from the candidate and reference genes. *ACT2* was used as a control.

ChIP assays

ChIP was performed as described previously (Bowler et al., 2004) with minor modifications to improve the enrichment (Lau and Bergmann, 2015). Plants were grown for 10 days under LD conditions, and approximately 9 g of seedlings was harvested at ZT12–ZT16. Plant tissue was crosslinked in a vacuum concentrator in the presence of 1 mM disuccinimidyl glutarate for 10 min, 1% (v/v) formaldehyde for 20 min, and 0.125 M glycine to stop crosslinking. The tissue was ground in liquid nitrogen, and chromatin was isolated. Chromatin complex immunoprecipitation was performed using an anti-CO antibody. After capturing immunocomplexes, they were eluted from the beads. The crosslinking between proteins and DNA was reversed, and the DNA was isolated. Subsequent qPCR was performed as described previously. Immunoprecipitated samples were normalized to a 10% reverse-crosslinked fraction of each chromatin preparation. The relative enrichment for each amplicon was normalized to that of the *ACT7* reference region. The primers used to measure DNA fragment enrichment in the ChIP experiments are shown in Supplemental Table 2.

RNA-seq and data analysis

Total RNA was extracted using an E.Z.N.A. Plant RNA Kit (Omega) from 10-day-old whole seedlings or petals following the manufacturer's instructions. Two independent biological replicates were processed for next-generation sequencing library preparation. Libraries were prepared using 250 ng of total RNA with the Illumina TruSeq Stranded mRNA protocol according to the manufacturer's instructions. Libraries were sequenced on an Illumina NextSeq 500 High Output by generating 1 × 75-bp single-end reads. Each biological sample from the different genotypes generated approximately 20 million single-end reads. Quality analysis was performed using FASTQC, and mapping against the reference genome TAIR10 from *A. thaliana* was done with HISAT2 (Kim et al., 2019). For transcript assembly and gene expression estimation in fragments per exon kilobase and million mapped reads, StringTie2 software and the R Bioconductor package Ballgown v.2.20 were used (Kovaka et al., 2019). Principal-component analysis for similarity analysis between replicates was performed using the R package FactoMineR v.2.33 (Lê et al., 2008). The differential gene expression analysis was performed using the Bioconductor R package limma v.3.444 (Ritchie et al., 2015). To determine upregulated and downregulated genes in ZT16 versus ZT4 a fold-change of ±2 and an adjusted p value of 0.05 were used, and exclusively a fold-change of ±1.5 was used for comparison between genotypes. The GO and Kyoto Encyclopedia of Genes and Genomes enrichment analyses were performed using the Bioconductor R package clusterProfiler v.3.165 (Yu et al., 2012). Data are available in the GEO NCBI database with accession number GSE204774.

Protein analysis

Arabidopsis proteins were isolated from petals or flowers at stage 14 of plants grown on peat-based compost using TRIzol (Invitrogen) as described by the manufacturer. To isolate *Nicotiana* proteins, 1 g of infected tissue was ground with a mortar and pestle in the presence of liquid nitrogen, resuspended in 2 ml of coIP buffer (Lazaro et al., 2012), and centrifuged for 10 min at 2350 *g* in a microfuge at 4°C. The amount of protein was determined by the Bradford assay (Bio-Rad) according to the manufacturer's instructions, using ovalbumin as a standard. Proteins were separated by SDS–PAGE using standard procedures, transferred to polyvinylidene difluoride filters, and probed with αCO (Serrano-Bueno et al., 2020), αGAPC (Valverde et al., 1999), αGFP (Proteintech), or αHA (Sigma–Aldrich, 12013819001). Blots were developed with a chemiluminescent substrate according to the manufacturer's instructions (Clarity Western ECL Substrate, Bio-Rad).

CoIP experiments were performed by transient assays in *N. benthamiana* cells (Serrano-Bueno et al., 2020). In brief, *Agrobacterium tumefaciens* GV3101 (pMP90) transformed with 35S:*3XHA*:*CO* (HA-CO), YFN:COI1, and YFC:JAZ3, were co-infiltrated into young leaves of *N. benthamiana* as described below. After 3 days, 1 g of infected tissue was ground as described below, and 0.5 ml of lysate was incubated with 25 μl of washed GFP-trap magnetic agarose beads (Chromotek, gtma-20) and stirred for 2 h at 4°C in a rotor incubator. After three washes in coIP buffer, samples were eluted by adding 5× SDS–PAGE loading buffer and incubating at 95°C for 5 min.

Microscopy

For BiFC experiments, *CO*, *COI1*, *JAZ*s, *MYC2*, and controls were cloned into pYFN43 and pYFC43 vectors (Ferrando et al., 2001) to produce N-terminal fusions of the carboxyl (pYFC43) and amino (pYFN43) parts of YFP. These constructs were introduced into *A. tumefaciens* strain C58 and infiltrated into *N. benthamiana* leaves together with p19 protein (Voinnet et al., 2003). The BiFC protocol was performed as described previously (Serrano-Bueno et al., 2020). The amino and carboxyl domains of AKINβ and AKIN10 sucrose-nonfermenting-related kinases were used as positive controls (Ferrando et al., 2001) or FKBP12 (Serrano-Bueno et al., 2020). FLM or empty vectors were used as negative controls. BiFC images were visualized under a Leica TCS SP2 confocal microscope set to 550 nm and analyzed with Leica LCSLite software.

For FRET experiments, reconstituted YFP (YFN:COI1/YFC:JAZ3) and CO-CFP constructs were introduced into *N. benthamiana* leaves by agroinfiltration. Two to three days after transfection, epidermal cells were visualized using a confocal laser scanning microscope (Olympus FV3000). CFP was excited with a 458-nm laser, and YFP was excited with a 514-nm laser. Band-pass filters were adjusted to 465–479 nm and 520–545 nm in the CFP and YFP detection channels, respectively. FRET was measured using the sensitized emission technique with preloaded Olympus software, and consequent analysis was performed using the PixFret plugin for ImageJ (Feige et al., 2005). The acceptor and donor bleedthrough was determined, the background was subtracted, and the N_{FRET} value was computed for each nucleus because this method normalizes differences in fluorescent protein levels (Feige et al., 2005).

Y2H

For Y2H assays, the CCT, middle, and b-box domains from CO were cloned into the bait vector pJG4-5, and the full-length

COI1, *JAZ3*, *JAZ9*, and *MYC2* coding sequences were cloned into the prey vector pEG202. The primers used to generate Y2H clones are listed in Supplemental Table 2. EGY48 (MAT*α trp1 ura3 his3 LEU2::pLex Aop6-LEU2*) was used as the host strain for Y2H experiments (Gyuris et al., 1993). Positive interactions were detected by blue dye on Ura–His–Trp X-gal plates and growth on GALGalactose–Ura–Trp–His–Leu ± coronatine-selective plates.

Site-directed mutagenesis

Site-directed mutagenesis was performed to replace the NIKY domain of CO according to the manufacturer's instructions (Muta-direct Site-Directed Mutagenesis, iNtRON Biotechnology). All constructs were verified by DNA sequencing. The primers used are listed in Supplemental Table 2.

Statistical analysis

The means ± SD from at least three biological experiments are shown. The statistical significance between means of the different samples was calculated using a two-tailed Student's *t*-test. Observed differences were considered statistically significant at $^{*}p < 0.05$, $^{**}p < 0.01$, and $^{***}p < 0.001$.

SUPPLEMENTAL INFORMATION

Supplemental information is available at *Molecular Plant Online*.

FUNDING

Authors would like to acknowledge the help or Drs. M. Calonje. And D. Pozo, and prof. M.A. Blazquez for critical reading of the manuscript. Work by G. S.-B. was supported by a European Union contract LONGFLOW (MSCAIF-2018-838317) and CSIC LONGFLOW (CONV_EXT_014). We also acknowledge financial support of from the Spanish Ministry for Science and Innovations (MICINN/FEDER) grants BIO2017-84066-R (to F.V.), PID2020-117018RB-I00 (to F.V.), and PID2019-107012RB-100 (to R.S. and A.C.).

AUTHOR CONTRIBUTIONS

G.S.-B., A.C., R.S., and F.V. designed the experimental approach. G.S.-B., P.d.l.R., V.S.d.M.-H., M.B., F.V., and A.C. performed most experiments. G.F.-G. and P.R. provided the RNA-seq and confocal analyseis. G.S., F.V., A.C., and R.S. wrote the paper. The final version of the manuscript was reviewed and revised by all authors.

ACKNOWLEDGMENTS

We acknowledge Drs. M. Calonje and D. Pozo and Prof. M.A. Blazquez for critical reading of the manuscript. No conflict of interest declared.

Received: May 24, 2022
Revised: September 8, 2022
Accepted: September 20, 2022
Published: September 23, 2022

REFERENCES

Acosta, I.F., and Przybyl, M. (2019). Jasmonate signaling during Arabidopsis stamen maturation. Plant Cell Physiol. **60**:2648–2659.

An, C., Li, L., Zhai, Q., You, Y., Deng, L., Wu, F., Chen, R., Jiang, H., Wang, H., Chen, Q., et al. (2017). Mediator subunit MED25 links the jasmonate receptor to transcriptionally active chromatin. Proc. Natl. Acad. Sci. USA **114**:E8930–E8939.

An, H., Roussot, C., Suárez-López, P., Corbesier, L., Vincent, C., Piñeiro, M., Hepworth, S., Mouradov, A., Justin, S., Turnbull, C., et al. (2004). CONSTANS acts in the phloem to regulate a systemic signal that induces photoperiodic flowering of Arabidopsis. Development **131**:3615–3626.

Ando, E., Ohnishi, M., Wang, Y., Matsushita, T., Watanabe, A., Hayashi, Y., Fujii, M., Ma, J.F., Inoue, S.i., and Kinoshita, T. (2013). TWIN SISTER OF FT, GIGANTEA, and CONSTANS have a positive but indirect effect on blue light-induced stomatal opening in Arabidopsis. Plant Physiol. **162**:1529–1538.

Andrés, F., and Coupland, G. (2012). The genetic basis of flowering responses to seasonal cues. Nat. Rev. Genet. **13**:627–639.

Austen, E.J., Rowe, L., Stinchcombe, J.R., and Forrest, J.R.K. (2017). Explaining the apparent paradox of persistent selection for early flowering. New Phytol. **215**:929–934.

Bleecker, A.B., and Patterson, S.E. (1997). Last exit: senescence, abscission, and meristem arrest in Arabidopsis. Plant Cell **9**:1169–1179.

Bowler, C., Benvenuto, G., Laflamme, P., Molino, D., Probst, A.V., Tariq, M., and Paszkowski, J. (2004). Chromatin techniques for plant cells. Plant J. **39**:776–789.

Chen, D., Yan, W., Fu, L.Y., and Kaufmann, K. (2018). Architecture of gene regulatory networks controlling flower development in *Arabidopsis thaliana*. Nat. Commun. **9**, 4534.

Chini, A., Fonseca, S., Fernández, G., Adie, B., Chico, J.M., Lorenzo, O., García-Casado, G., López-Vidriero, I., Lozano, F.M., Ponce, M.R., et al. (2007). The JAZ family of repressors is the missing link in jasmonate signalling. Nature **448**:666–671.

Chini, A., Fonseca, S., Chico, J.M., Fernández-Calvo, P., and Solano, R. (2009). The ZIM domain mediates homo- and heteromeric interactions between Arabidopsis JAZ proteins. Plant J. **59**:77–87.

Chini, A., Gimenez-Ibanez, S., Goossens, A., and Solano, R. (2016). Redundancy and specificity in jasmonate signalling. Curr. Opin. Plant Biol. **33**:147–156.

Chung, H.S., and Howe, G.A. (2009). A critical role for the TIFY motif in repression of jasmonate signaling by a stabilized splice variant of the JASMONATE ZIM-domain protein JAZ10 in Arabidopsis. Plant Cell **21**:131–145.

Deng, X., Fan, X., Li, P., and Fei, X. (2015). A photoperiod-regulating gene *CONSTANS* is correlated to lipid biosynthesis in *Chlamydomonas reinhardtii*. BioMed Res. Int.715020

Dhar, N., Caruana, J., Erdem, I., Subbarao, K.V., Klosterman, S.J., and Raina, R. (2020). The Arabidopsis SENESCENCE-ASSOCIATED GENE 13 regulates dark-induced senescence and plays contrasting roles in defense against bacterial and fungal pathogens. Mol. Plant Microbe Interact. **33**:754–766.

Ettinger, A.K., Buonaiuto, D.M., Chamberlain, C.J., Morales-Castilla, I., and Wolkovich, E.M. (2021). Spatial and temporal shifts in photoperiod with climate change. New Phytol. **230**:462–474.

Fang, C., Zhang, H., Wan, J., Wu, Y., Li, K., Jin, C., Chen, W., Wang, S., Wang, W., Zhang, H., et al. (2016). Control of leaf senescence by an MeOH-jasmonates cascade that is epigenetically regulated by OsSRT1 in rice. Mol. Plant **9**:1366–1378.

Fernández-Calvo, P., Chini, A., Fernández-Barbero, G., Chico, J.M., Gimenez-Ibanez, S., Geerinck, J., Eeckhout, D., Schweizer, F., Godoy, M., Franco-Zorrilla, J.M., et al. (2011). The Arabidopsis bHLH transcription factors MYC3 and MYC4 are targets of JAZ repressors and act additively with MYC2 in the activation of jasmonate responses. Plant Cell **23**:701–715.

Gyuris, J., Golemis, E., Chertkov, H., and Brent, R. (1993). Cdi1, a human G1and S phase protein phosphatase that associates with Cdk2. Cell **75**:791–803.

Feige, J.N., Sage, D., Wahli, W., Desvergne, B., and Gelman, L. (2005). PixFRET, an ImageJ plug-in for FRET calculation that can accommodate variations in spectral bleed-throughs. Microsc. Res. Tech. **68**:51–58.

Ferrando, A., Koncz-Kálmán, Z., Farràs, R., Tiburcio, A., Schell, J., and Koncz, C. (2001). Detection of in vivo protein interactions between Snf1-related kinase subunits with intron-tagged epitope-labelling in plants cells. Nucleic Acids Res. **29**:3685–3693.

Fonseca, S., Chini, A., Hamberg, M., Adie, B., Porzel, A., Kramell, R., Miersch, O., Wasternack, C., and Solano, R. (2009). (+)-7-iso-Jasmonoyl-L-isoleucine is the endogenous bioactive jasmonate. Nat. Chem. Biol. **5**:344–350.

Gabilly, S.T., Baker, C.R., Wakao, S., Crisanto, T., Guan, K., Bi, K., Guiet, E., Guadagno, C.R., and Niyogi, K.K. (2019). Regulation of photoprotection gene expression in *Chlamydomonas* by a putative E3 ubiquitin ligase complex and a homolog of *CONSTANS*. Proc. Natl. Acad. Sci. USA **116**:17556–17562.

Heo, J.W., Chakrabarty, D., and Paek, K.Y. (2004). Longevity and quality of cut 'Master' carnation and 'Red Sandra' rose flowers as affected by red light. Plant Growth Regul. **42**:169–174.

Hou, X., Lee, L.Y.C., Xia, K., Yan, Y., and Yu, H. (2010). DELLAs modulate jasmonate signaling via competitive binding to JAZs. Dev. Cell **19**:884–894.

Howe, G.A., Major, I.T., and Koo, A.J. (2018). Modularity in jasmonate signaling for multistress resilience. Annu. Rev. Plant Biol. **69**:387–415.

Hu, Y., Jiang, Y., Han, X., Wang, H., Pan, J., and Yu, D. (2017). Jasmonate regulates leaf senescence and tolerance to cold stress: crosstalk with other phytohormones. J. Exp. Bot. **68**:1361–1369.

Jewell, J.B., and Browse, J. (2016). Epidermal jasmonate perception is sufficient for all aspects of jasmonate-mediated male fertility in Arabidopsis. Plant J. **85**:634–647.

Jibran, R., A Hunter, D., and P Dijkwel, P. (2013). Hormonal regulation of leaf senescence through integration of developmental and stress signals. Plant Mol. Biol. **82**:547–561.

Kazan, K. (2015). Diverse roles of jasmonates and ethylene in abiotic stress tolerance. Trends Plant Sci. **20**:219–229.

Kim, D., Paggi, J.M., Park, C., Bennett, C., and Salzberg, S.L. (2019). Graph-based genome alignment and genotyping with HISAT2 and HISAT-genotype. Nat. Biotechnol. **37**:907–915.

Kinoshita, A., and Richter, R. (2020). Genetic and molecular basis of floral induction in *Arabidopsis thaliana*. J. Exp. Bot. **71**:2490–2504.

Körner, C., and Basler, D. (2010). Phenology under global warming. Science **327**:1461–1462.

Thomas, H. (2013). Senescence, ageing and death of the whole plant. New Phytol. **197**:696–711.

Kovaka, S., Zimin, A.V., Pertea, G.M., Razaghi, R., Salzberg, S.L., and Pertea, M. (2019). Transcriptome assembly from long-read RNA-seq alignments with StringTie2. Genome Biol. **20**:278.

Lau, O.S., and Bergmann, D.C. (2015). MOBE-ChIP: a large-scale chromatin immunoprecipitation assay for cell type-specific studies. Plant J. **84**:443–450.

Lazaro, A., Valverde, F., Piñeiro, M., and Jarillo, J.A. (2012). The Arabidopsis E3 ubiquitin ligase HOS1 negatively regulates CONSTANS abundance in the photoperiodic control of flowering. Plant Cell **24**:982–999.

Lazaro, A., Mouriz, A., Piñeiro, M., and Jarillo, J.A. (2015). Red light-mediated degradation of CONSTANS by the E3 ubiquitin ligase HOS1 regulates photoperiodic flowering in Arabidopsis. Plant Cell **27**:2437–2454.

Lê, S., Josse, j., and Husson, F. (2008). FactoMineR: an R package for multivariate analysis. J. Stat. Softw. **25**:1–18.

Liu, L.J., Zhang, Y.C., Li, Q.H., Sang, Y., Mao, J., Lian, H.L., Wang, L., and Yang, H.Q. (2008). COP1-Mediated ubiquitination of CONSTANS is implicated in cryptochrome regulation of flowering in Arabidopsis. Plant Cell **20**:292–306.

Lorenzo, O., Chico, J.M., Sánchez-Serrano, J.J., and Solano, R. (2004). JASMONATE-INSENSITIVE1 encodes a MYC transcription factor essential to discriminate between different jasmonate-regulated defense responses in Arabidopsis. Plant Cell **16**:1938–1950.

Mandaokar, A., Thines, B., Shin, B., Lange, B.M., Choi, G., Koo, Y.J., Yoo, Y.J., Choi, Y.D., Choi, G., and Browse, J. (2006). Transcriptional regulators of stamen development in Arabidopsis identified by transcriptional profiling. Plant J. **46**:984–1008.

Mandaokar, A., and Browse, J. (2009). MYB108 acts together with MYB24 to regulate jasmonate-mediated stamen maturation in Arabidopsis. Plant Physiol. **149**:851–862.

Manfield, I.W., Devlin, P.F., Jen, C.H., Westhead, D.R., and Gilmartin, P.M. (2007). Conservation, convergence, and divergence of light-responsive, circadian-regulated, and tissue-specific expression patterns during evolution of the Arabidopsis GATA gene family. Plant Physiol. **143**:941–958.

Maor, R., Jones, A., Nühse, T.S., Studholme, D.J., Peck, S.C., and Shirasu, K. (2007). Multidimensional protein identification technology (MudPIT) analysis of ubiquitinated proteins in plants. Mol. Cell. Proteomics **6**:601–610.

Ortiz-Marchena, M.I., Albi, T., Lucas-Reina, E., Said, F.E., Romero-Campero, F.J., Cano, B., Ruiz, M.T., Romero, J.M., and Valverde, F. (2014). Photoperiodic control of carbon distribution during the floral transition in Arabidopsis. Plant Cell **26**:565–584.

Park, J.H., Halitschke, R., Kim, H.B., Baldwin, I.T., Feldmann, K.A., and Feyereisen, R. (2002). A knock-out mutation in allene oxide synthase results in male sterility and defective wound signal transduction in Arabidopsis due to a block in jasmonic acid biosynthesis. Plant J. **31**:1–12.

Qi, T., Huang, h., Song, S., and Xie, D. (2015). Regulation of jasmonate-mediated stamen development and seed production by a bHLH-MYB complex in Arabidopsis. Plant Cell **27**:1620–1633.

Ritchie, M.E., Phipson, B., Wu, D., Hu, Y., Law, C.W., Shi, W., and Smyth, G.K. (2015). Limma powers differential expression analyses for RNA-sequencing and microarray studies. Nucleic Acids Res. **43**:e47.

Robson, F., Costa, M.M., Hepworth, S.R., Vizir, I., Piñeiro, M., Reeves, P.H., Putterill, J., and Coupland, G. (2001). Functional importance of conserved domains in the flowering-time gene CONSTANS demonstrated by analysis of mutant alleles and transgenic plants. Plant J. **28**:619–631.

Robson, F., Okamoto, H., Patrick, E., Harris, S.R., Wasternack, C., Brearley, C., and Turner, J.G. (2010). Jasmonate and phytochrome A signaling in Arabidopsis wound and shade responses are Integrated through JAZ1 stability. Plant Cell **22**:1143–1160.

Ruijter, J.M., Ramakers, C., Hoogaars, W.M.H., Karlen, Y., Bakker, O., van den Hoff, M.J.B., and Moorman, A.F.M. (2009). Amplification efficiency: linking baseline and bias in the analysis of quantitative PCR data. Nucleic Acids Res. **37**:e45.

Sakuraba, Y. (2021). Light-mediated regulation of leaf senescence. Int. J. Mol. Sci. **22**, 3291.

Samach, A., Onouchi, H., Gold, S.E., Ditta, G.S., Schwarz-Sommer, Z., Yanofsky, M.F., and Coupland, G. (2000). Distinct roles of CONSTANS target genes in reproductive development of Arabidopsis. Science **288**:1613–1616.

Saracco, S.A., Hansson, M., Scalf, M., Walker, J.M., Smith, L.M., and Vierstra, R.D. (2009). Tandem affinity purification and mass spectrometric analysis of ubiquitylated proteins in Arabidopsis. Plant J. **59**:344–358.

Serrano-Bueno, G., Romero-Campero, F.J., Lucas-Reina, E., Romero, J.M., and Valverde, F. (2017). Evolution of photoperiod sensing in plants and algae. Curr. Opin. Plant Biol. **37**:10–17.

Serrano-Bueno, G., Said, F.E., de Los Reyes, P., Lucas-Reina, E.I., Ortiz-Marchena, M.I., Romero, J.M., and Valverde, F. (2020). CONSTANS–FKBP12 interaction contributes to modulation of photoperiodic flowering in Arabidopsis. Plant J. **101**:1287–1302.

Serrano-Bueno, G., Sánchez de Medina Hernández, V., and Valverde, F. (2021). Photoperiodic signaling and senescence, an ancient solution to a modern problem? Front. Plant Sci. **12**, 634393. https://doi.org/10.3389/fpls.2021.634393.

Sheard, L.B., Tan, X., Mao, H., Withers, J., Ben-Nissan, G., Hinds, T.R., Kobayashi, Y., Hsu, F.F., Sharon, M., Browse, J., et al. (2010). Sheng Yang He, Josep Rizo, Gregg A Howe, Ning Zheng, jasmonate perception by inositol-phosphate-potentiated COI1-JAZ co-receptor. Nature **468**:400–405.

Simon, R., Igeño, M.I., and Coupland, G. (1996). Activation of floral meristem identity genes in Arabidopsis. Nature **384**:59–62.

Song, S., Qi, T., Huang, H., Ren, Q., Wu, D., Chang, C., Peng, W., Liu, Y., Peng, J., and Xie, D. (2011). The Jasmonate-ZIM domain proteins interact with the R2R3-MYB transcription factors MYB21 and MYB24 to affect Jasmonate-regulated stamen development in Arabidopsis. Plant Cell **23**:1000–1013.

Suárez-López, P., Wheatley, K., Robson, F., Onouchi, H., Valverde, F., and Coupland, G. (2001). CONSTANS mediates between the circadian clock and the control of flowering in Arabidopsis. Nature **410**:1116–1120.

Thines, B., Katsir, L., Melotto, M., Niu, Y., Mandaokar, A., Liu, G., Nomura, K., He, S.Y., Howe, G.A., and Browse, J. (2007). JAZ repressor proteins are targets of the SCF(COI1) complex during jasmonate signalling. Nature **448**:661–665.

Tiwari, S.B., Shen, Y., Chang, H.C., Hou, Y., Harris, A., Ma, S.F., McPartland, M., Hymus, G.J., Adam, L., Marion, C., et al. (2010). The flowering time regulator CONSTANS is recruited to the FLOWERING LOCUS T promoter via a unique cis-element. New Phytol. **187**:57–66.

Tokutsu, R., Fujimura-Kamada, K., Matsuo, T., Yamasaki, T., and Minagawa, J. (2019). The CONSTANS flowering complex controls the protective response of photosynthesis in the green alga Chlamydomonas. Nat. Commun. **10**, 4099.

Valverde, F., Losada, M., and Serrano, A. (1999). Engineering a central metabolic pathway: glycolysis with no net phosphorylation in an *Escherichia coli gap* mutant complemented with a plant *GapN* gene. FEBS Lett. **449**:153–158.

Valverde, F., Mouradov, A., Soppe, W., Ravenscroft, D., Samach, A., and Coupland, G. (2004). Photoreceptor regulation of CONSTANS protein in photoperiodic flowering. Science **303**:1003–1006.

Valverde, F. (2011). CONSTANS and the evolutionary origin of photoperiodic timing of flowering. J. Exp. Bot. **62**:2453–2463.

Voinnet, O., Rivas, S., Mestre, P., and Baulcombe, D. (2003). An enhanced transient expression system in plants based on suppression of gene silencing by the p19 protein of tomato bushy stunt virus. Plant J. **33**:949–956.

Wasternack, C., and Feussner, I. (2018). The Oxylipin pathways: biochemistry and function. Annu. Rev. Plant Biol. **69**:363–386.

Wellmer, F., Alves-Ferreira, M., Dubois, A., Riechmann, J.L., and Meyerowitz, E.M. (2006). Genome-wide analysis of gene expression during early Arabidopsis flower development. PLoS Genet. **2**, e117.

Xia, Z., and Liu, Y. (2001). Reliable and global measurement of fluorescence resonance Energy transfer using fluorescence microscopes. Biophys. J. **81**:2395–2402.

Xie, D.X., Feys, B.F., James, S., Nieto-Rostro, M., and Turner, J.G. (1998). COI1: an Arabidopsis gene required for jasmonate-regulated defense and fertility. Science **280**:1091–1094.

Yin, J., Chang, X., Kasuga, T., Bui, M., Reid, M.S., and Jiang, C.Z. (2015). A basic helix-loop-helix transcription factor, PhFBH4, regulates flower senescence by modulating ethylene biosynthesis pathway in petunia. Hortic. Res. **2**, 15059.

Yoo, S.K., Chung, K.S., Kim, J., Lee, J.H., Hong, S.M., Yoo, S.J., Yoo, S.Y., Lee, J.S., and Ahn, J.H. (2005). CONSTANS activates *SUPPRESSOR OF OVEREXPRESSION OF CONSTANS 1* through *FLOWERING LOCUS T* to promote flowering in Arabidopsis. Plant Physiol. **139**:770–778.

Yu, G., Wang, L.G., Han, Y., and He, Q.Y. (2012). ClusterProfiler: an R package for comparing biological themes among gene clusters. Omi. A J. Integr. Biol. **16**:284–287.

Zander, M., Lewsey, M.G., Clark, N.M., Yin, L., Bartlett, A., Saldierna Guzmán, J.P., Hann, E., Langford, A.E., Jow, B., Wise, A., et al. (2020). Integrated multi-omics framework of the plant response to jasmonic acid. Nat. Plants **6**:290–302.

Zhai, Q., Zhang, X., Wu, F., Feng, H., Deng, L., Xu, L., Zhang, M., Wang, Q., and Li, C. (2015). Transcriptional mechanism of jasmonate receptor COI1-mediated delay of flowering time in Arabidopsis. Plant Cell **27**:2814–2828.

Zhai, Q., Deng, L., and Li, C. (2020). Mediator subunit MED25: at the nexus of jasmonate signalling. Curr. Opin. Plant Biol. **57**:78–86.

Molecular Plant, Volume *15*

Supplemental information

Regulation of floral senescence in *Arabidopsis* by coordinated action of *CONSTANS* and jasmonate signaling

Gloria Serrano-Bueno, Pedro de los Reyes, Andrea Chini, Gabriel Ferreras-Garrucho, Víctor Sánchez de Medina-Hernández, Marta Boter, Roberto Solano, and Federico Valverde

SUPPLEMENTAL INFORMATION

Regulation of floral senescence in Arabidopsis by coordinated action of *CONSTANS* and jasmonate signaling

Gloria Serrano-Bueno[1]*, Pedro de los Reyes[1†], Andrea Chini[2], Gabriel Ferreras-Garrucho[1,3], Víctor Sánchez de Medina-Hernández[1,4], Marta Boter[2], Roberto Solano[2], and Federico Valverde[1]*.

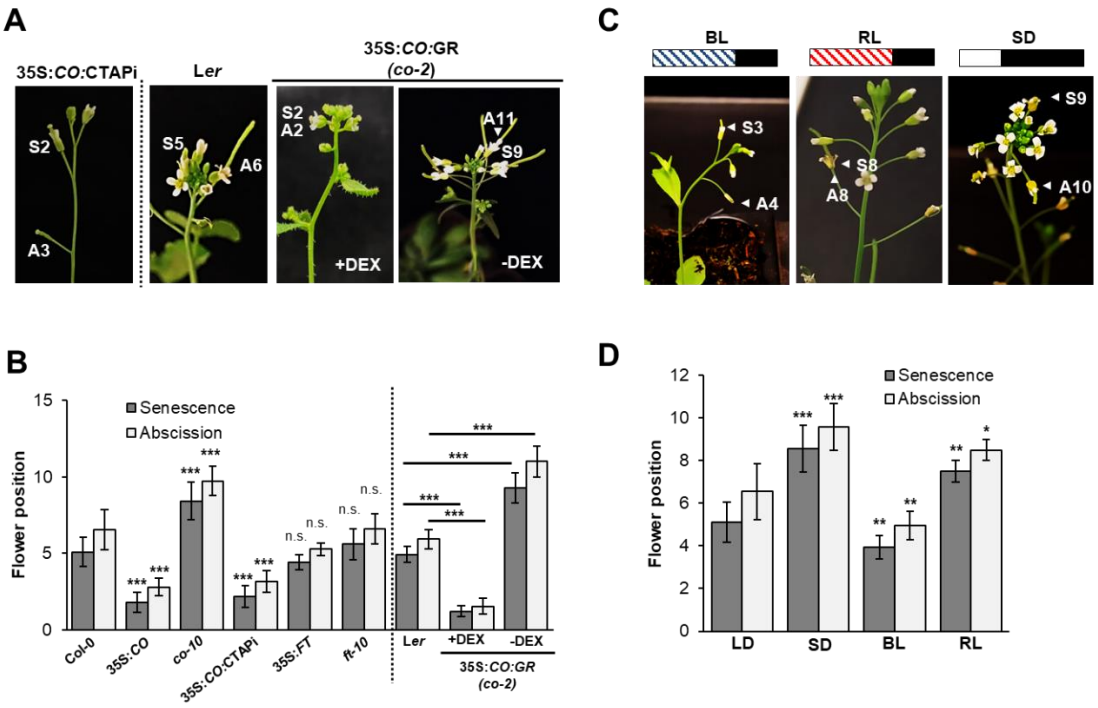

Supplementary Fig. S1 Light quality and photoperiod affect flower senescence and abscission.

(A) Flower senescence and abscission phenotypes of 35S:*CO*:CTAPi, L*er* and 35S:*CO*:GR (*co-2*) plants. 35S:*CO*:GR (*co-2*) plants were left untreated (-DEX) or treated (+DEX) with the steroid dexamethasone (10 µM, once per week) **(B)** Position of flowers showing yellowing (dark grey bars) and abscission (light grey bars) in Col-0, 35S:*CO*, *co-10*, 35S:*CO*:CTAPi, 35S:*FT*, *ft-10*, L*er* and 35S:*CO*:GR (*co-2*) +/-DEX plants. Error bars indicate s.d. of > 50 inflorescences **(C)** Flower senescence and abscission phenotypes of WT plants grown under SD, BL and RL **(D)** Position of flowers showing yellowing (dark grey bars) and abscission (light grey bars) in WT plants grown under LD, SD, BL and RL. Error bars indicate s.d. of > 50 inflorescences

Supplementary Fig. S2 Detailed flower senescence and abscission in WT, 35S:*CO*, *co-10*, *aos1-1* and 35S:*CO aos1-1* plants.

(A) Set up of cut flowers from different developmental stages showing differences in senescence and abscission **(B)** Examples of detailed pictures of flower stem insertion position for senescence and abscission count. Arrows indicate the flowers used for quantifying senescence and abscission.

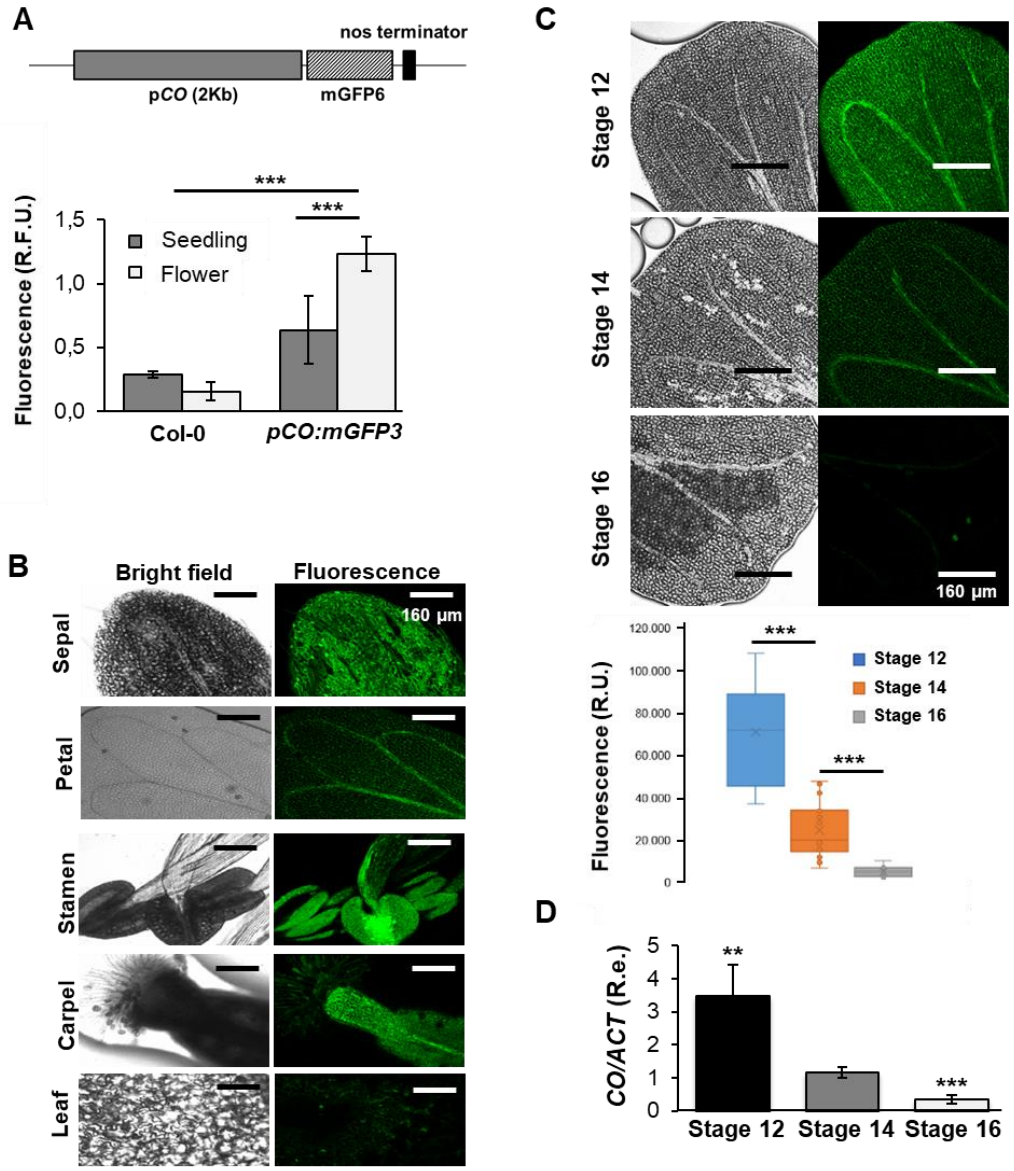

Supplementary Fig. S3 *CO* promoter activity in *Arabidopsis* flowers.

(A) Schematic diagram of the p*CO*:*mGFP6* reporter used in this study. Bottom, fluorescence measure of *Arabidopsis* transgenic lines expressing p*CO*:*mGFP6*. WT plants were used as control. Light grey, flowers. Dark grey, seedlings **(B)** Epidermal cells of floral organs (sepal, petal, stamen, carpel) and leaf of *Arabidopsis* transgenic lines expressing p*CO*:*mGFP6*. Left panels, bright field, right panels GFP fluorescence. Scale bar represents 160 µm **(C)** Epidermal cells of p*CO*:*mGFP6* petals in different developmental stages, LD, ZT16 (12, 14 and 16 days). Bottom panel, fluorescence activity of *Arabidopsis* petals expressing p*CO*:*mGFP6* in Stages 12, 14 and 16, LD, ZT16. Error bars, s.d. >50 petals **(D)** RT-qPCR analyses of *CO* expression in WT petals in Stages 12, 14 and 16, LD, ZT16. *ACT2* as control. Error bars, s.d. from three independent experiments. Asterisks indicate significance, ** p<0.01, *** p<0.001.

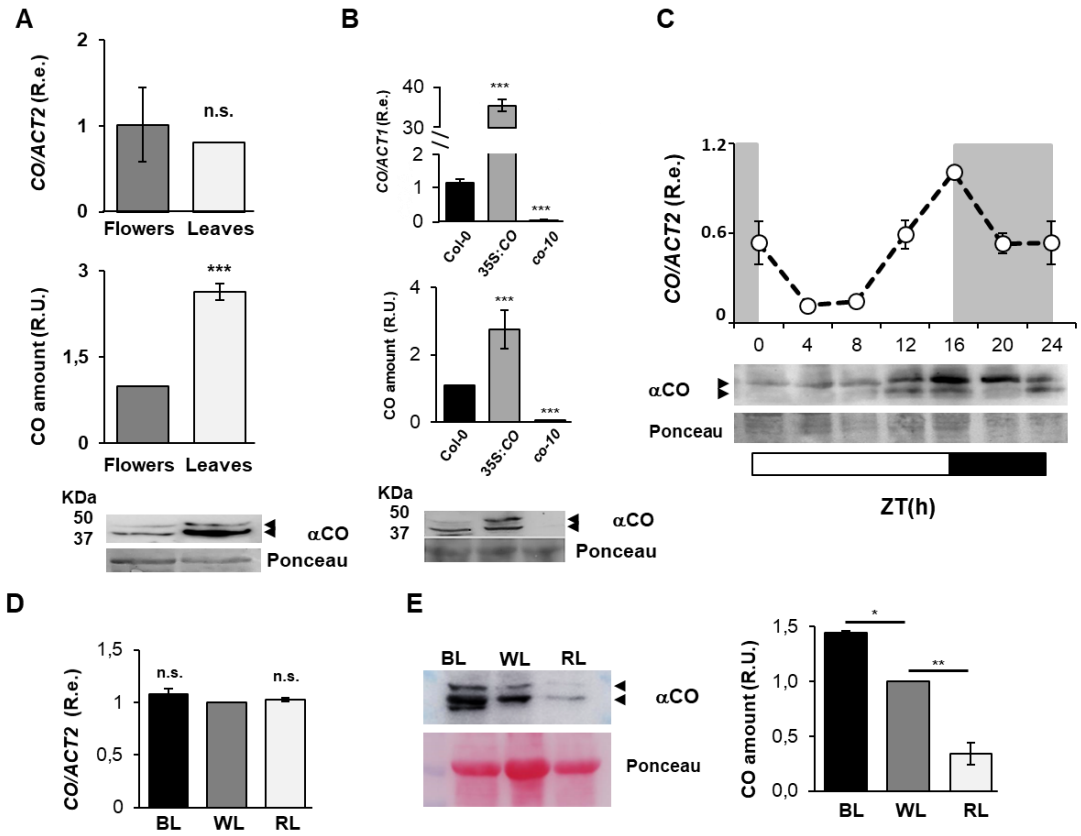

Supplementary Fig. S4 Correlation between floral CO protein accumulation and flower senescence and abscission.

(A) (Top), RT-qPCR analyses of *CO* expression in WT flowers and leaves, LD, ZT16. *ACT2* was used as a control. Error bars, s.d. from three independent experiments. (Bottom), αCO Immunoblot showing CO accumulation in WT flowers and leaves, LD, ZT16 and quantification of protein levels in three replicates. Ponceau staining as control. Error bars, s.d. from three independent experiments **(B)** (Top), RT-qPCR analyses of *CO* expression in WT, 35S:*CO* and *co-10* flowers, LD, ZT16. *ACT2* was as control. Error bars, s.d. from three independent experiments. (Bottom), αCO Immunoblot showing CO accumulation in WT, 35S:*CO* and *co-10* flowers, LD, ZT16 and quantification of protein levels in three. Ponceau staining as loading control **(C)** (Top), time course RT-qPCR analysis of *CO* expression in WT seedlings, LD. *ACT2* as control. Error bars, s.d. from three independent experiments. (Bottom), αCO immunoblots showing 24h accumulation of CO in WT seedlings, LD **(D)** RT-qPCR analyses of *CO* expression in WT flowers grown under WL, BL and RL, LD, ZT16. *ACT2* as control. Error bars, s.d. from three independent experiments **(E)** Left, αCO immunoblot showing CO accumulation in WT flowers grown under WL, BL and RL, LD, ZT16. Right, quantification of protein levels in three replicates by Western blot using αCO. Ponceau staining served as loading control. Error bars, s.d. from three independent experiments.

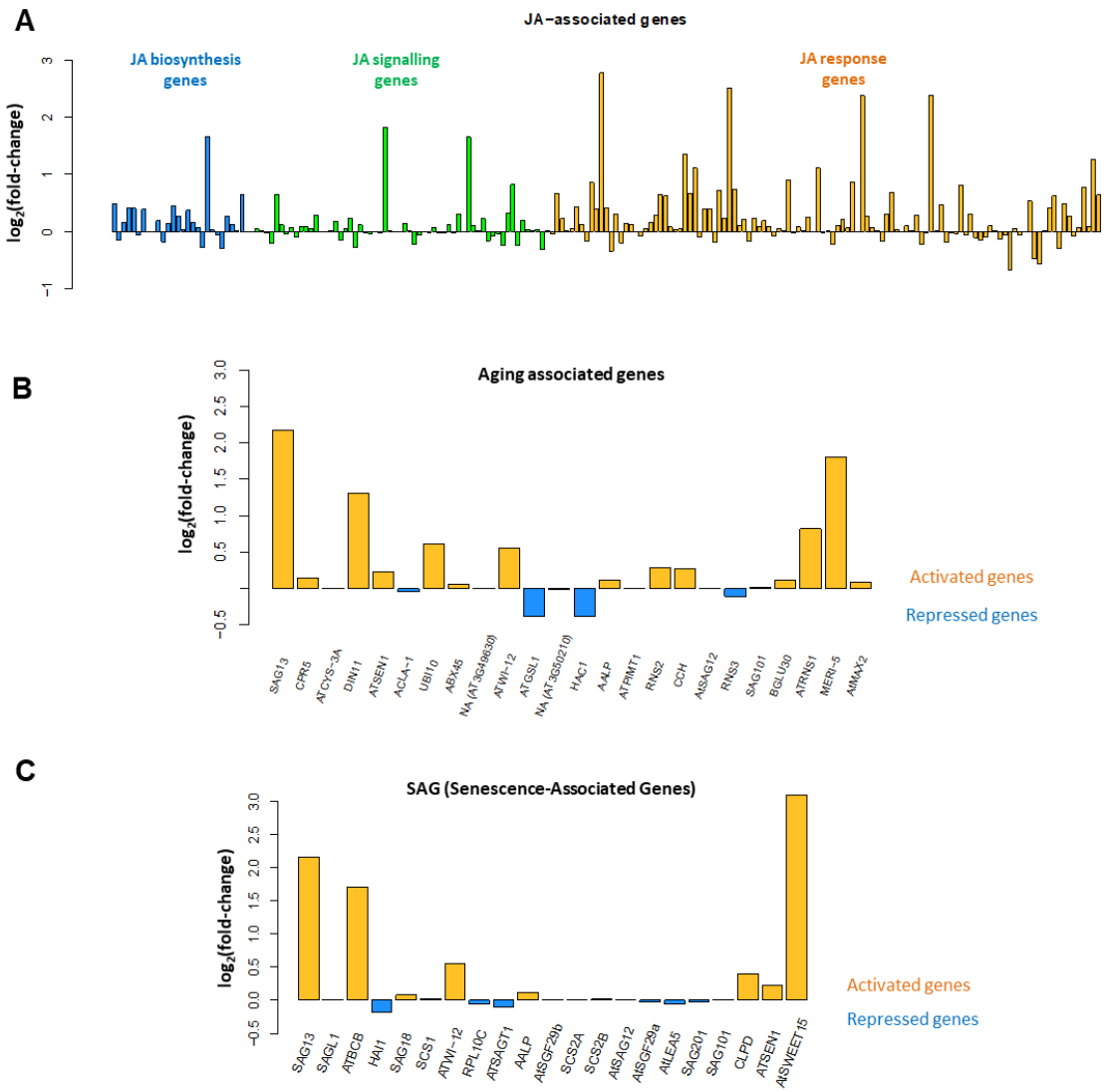

Supplementary Fig. S5 Jasmonate, aging and senescence associated genes are up-regulated in 35S:*CO* seedlings.

(A) Diagram of fold-changes (logarithmic) showing JA-associated genes expression in 35S:*CO* vs WT pairwise comparison in seedlings, LD, ZT16 **(B)** Diagram of fold-changes (logarithmic) of aging-associated genes expression in 35S:*CO* vs WT pairwise comparison in seedlings, LD, ZT16 **(C)** Diagram of fold-changes (logarithmic) of *SAGs* (*Senescence-Associated Genes*) in 35S:*CO* vs WT pairwise comparison in seedlings, LD, ZT16. A list of the upregulated genes can be found in Table S1. See also Supplementary Data 1, 2.

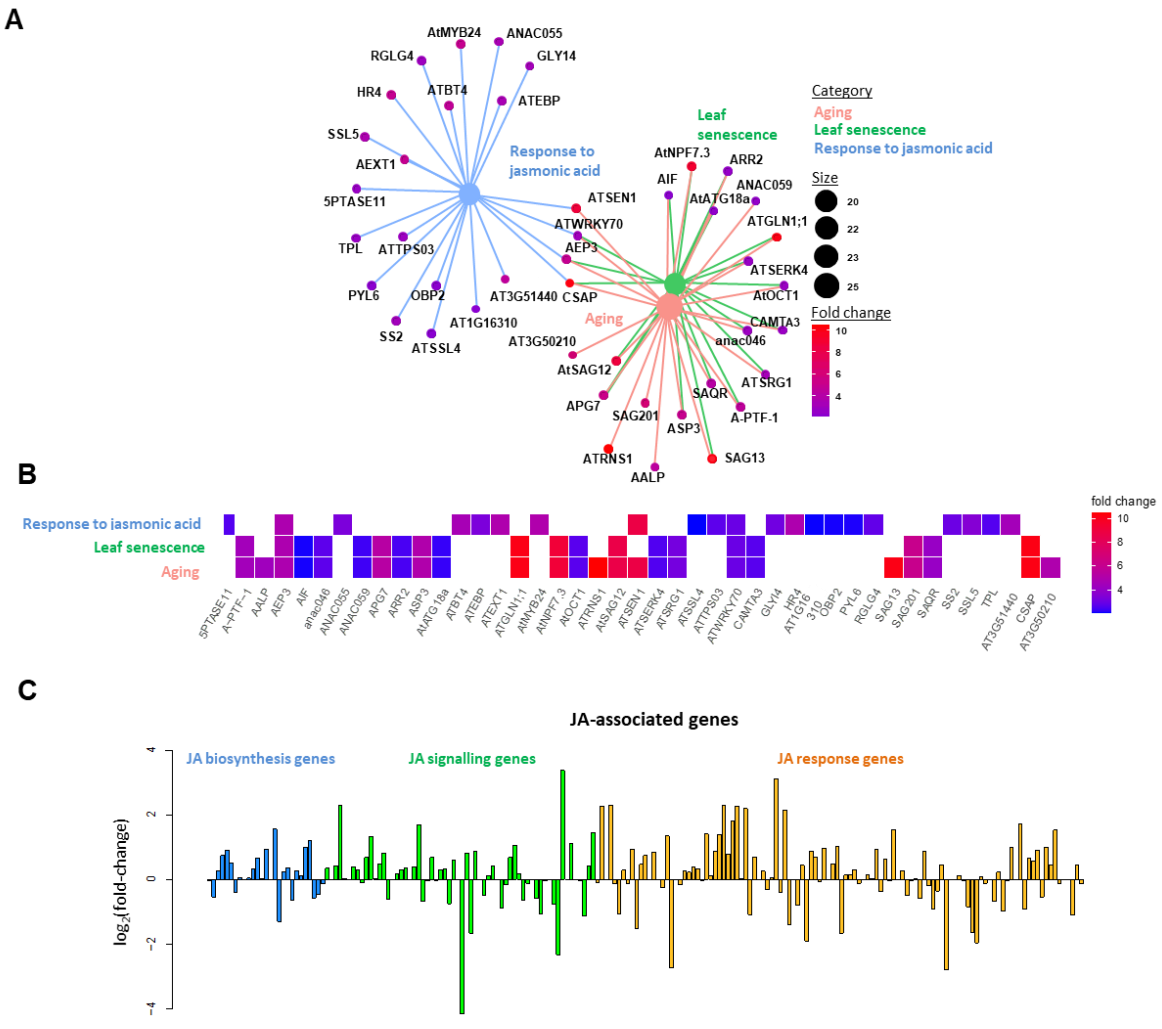

76

77 **Supplementary Fig. S6 Jasmonate, aging and senescence associated genes are**
78 **up-regulated during the afternoon in WT petals.**

79 **(A) (B)** GO enrichment analysis of up-regulated genes in the ZT16 vs ZT4 pairwise
80 comparison in WT petals. Diagrams show GO terms of interest and associated
81 differentially expressed genes (DEGs), with corresponding fold-changes **(C)** Diagram of
82 fold-changes (logarithmic) of JA-associated genes expression in the WT petals ZT16 vs
83 ZT4 comparison. See also Supplementary Data 1, 2.

84

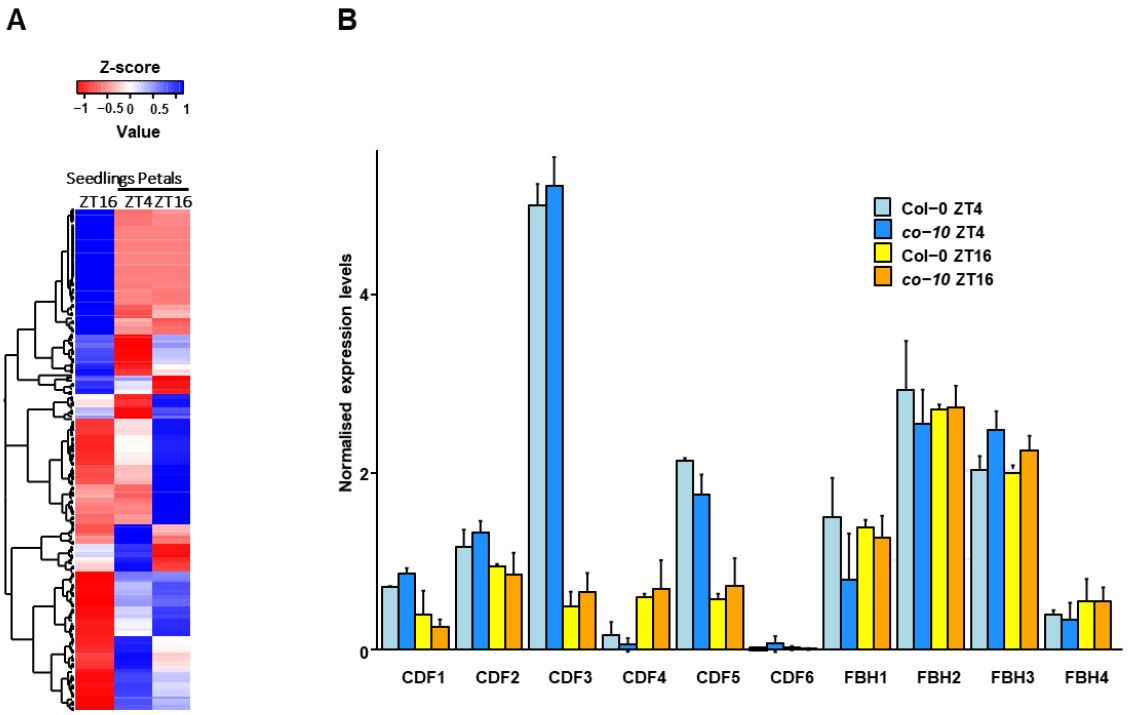

Supplementary Fig. S7. Normalized expression of JA- and photoperiod-associated genes.

(A) Heatmap of normalized expression levels of JA-associated genes in WT seedlings ZT16, petals ZT4 and petals ZT16. Notice how the activated or repressed genes show an almost opposing expression **(B)** Normalized expression levels of photoperiodic flowering-associated genes (*CDFs* and *FBHs*) in WT and *co-10* petals, ZT4 and ZT16. See also Supplementary Data 1, 2.

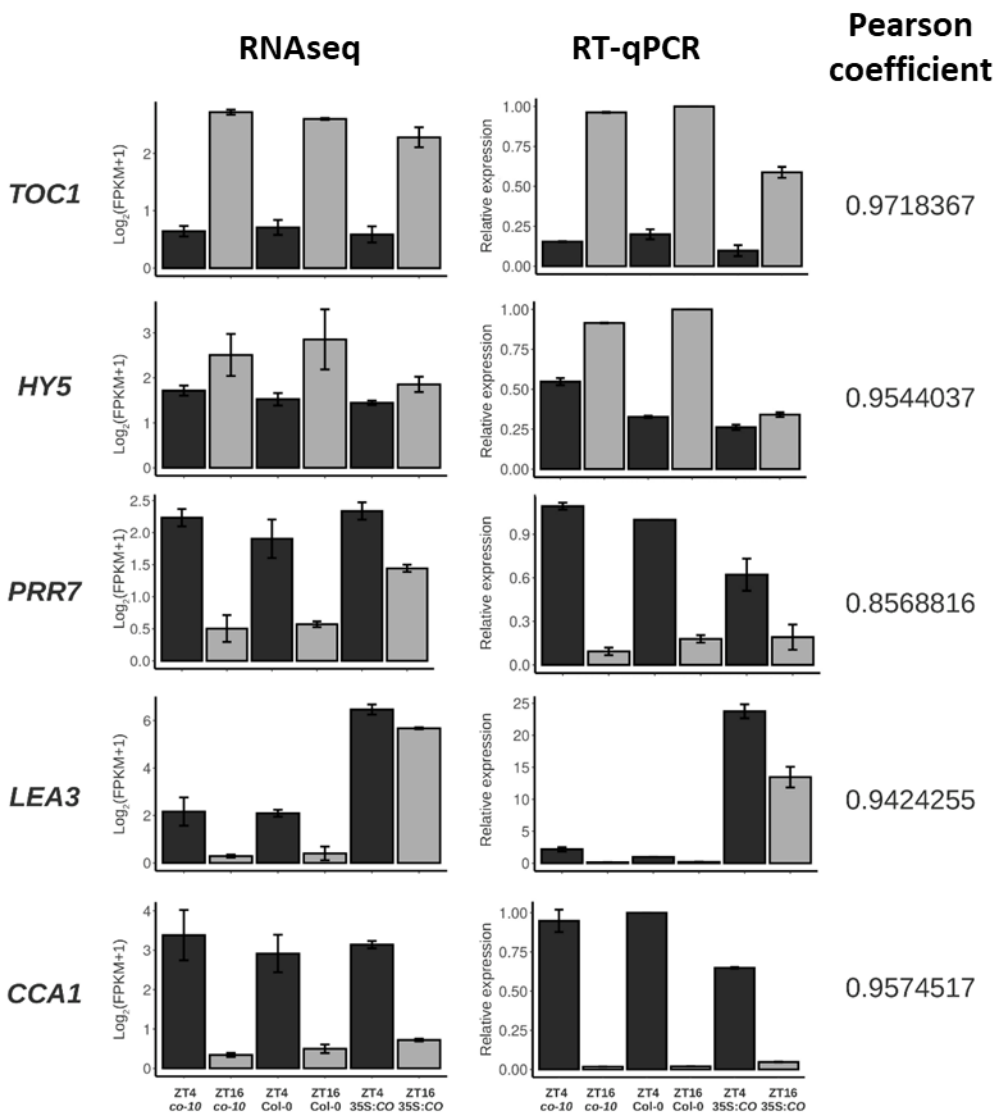

Supplementary Fig. S8. RNAseq validation by real-time qPCR (RT-qPCR).

Five genes showing differential expression between some samples were randomly selected confirm the RNAseq data (*TOC1, HY5*, *PRR7*, *LEA3*, and *CCA1*). *UBQ10* gene was used as housekeeping. The normalized expression from RNAseq data is represented in the first column and the relative expression resulting from RT-qPCR experiments is plotted in the second column. The Pearson correlation was calculated between the RNAseq data values (FPKM) and RT-qPCR values (relative expression) across all conditions.

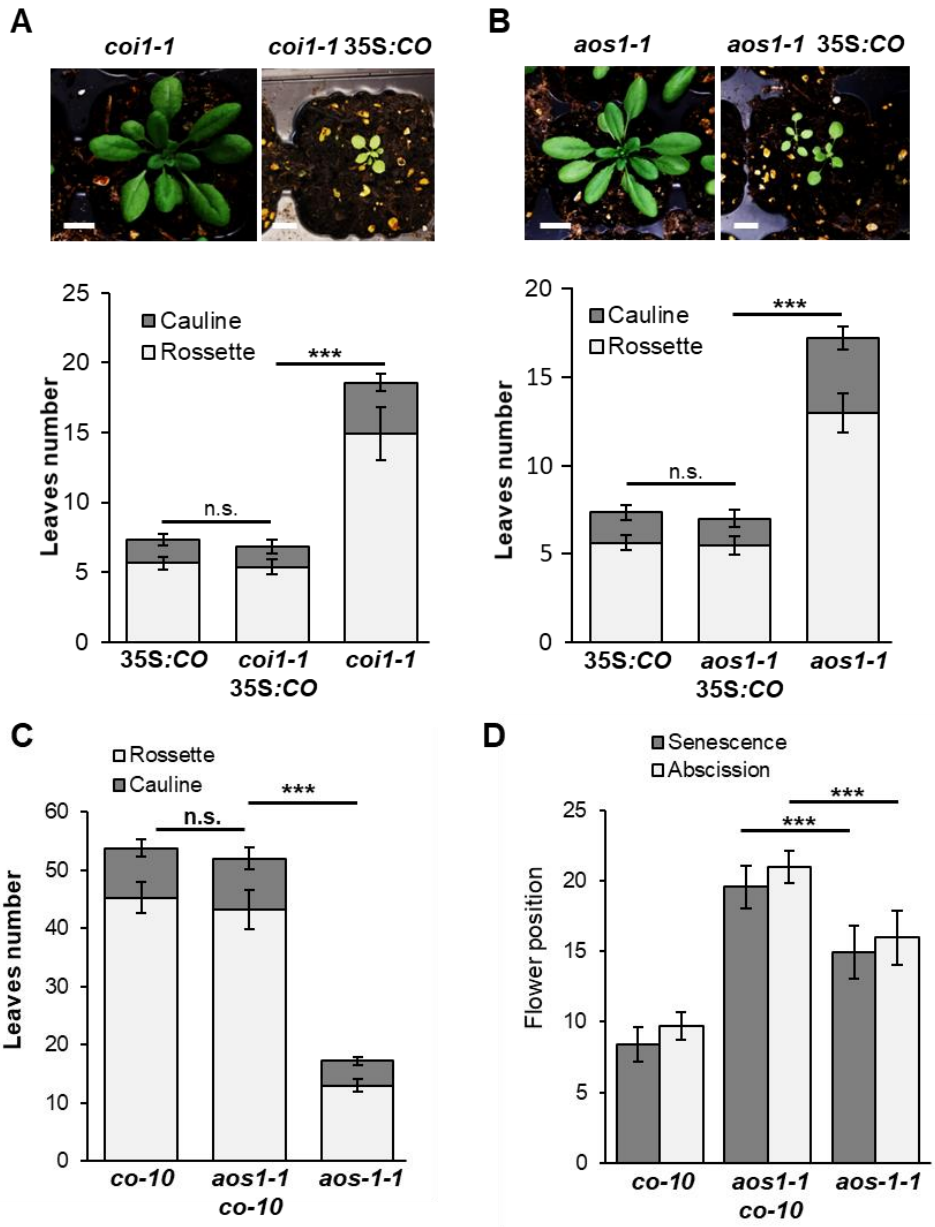

112

113 **Supplementary Fig. S9 Phenotype of *aos1-1* 35S:*CO*, *coi1-1* 35S:*CO*, and *aos1-1***
114 ***co-10* crosses.**

115 **(A)** (Top), flowering phenotype of *coi1-1* and *coi1-1* 35S:*CO* in LD. (Bottom), flowering
116 time measure. Light grey bars, rosette leaves; dark grey bars, cauline leaves. Error bars,
117 s.d. of > 50 plants **(B)** (Top), flowering phenotype of *aos1-1* and *aos1-1* 35S:*CO* in LD.
118 (Bottom), flowering time measurement; light grey bars, rosette leaves; dark grey bars,
119 cauline leaves. Error bars, s.d. > 50 plants. **(C)** Flowering time measure of *aos1-1 co-10*
120 in LD. Light grey bars, rosette leaves; dark grey bars, cauline leaves. Error bars, s.d. of
121 > 50 plants. **(D)** Position of flowers showing yellowing (dark grey bars) and abscission
122 (light grey bars) in *aos1-1 co-10* plants grown under LD. Error bars indicate s.d. of > 50
123 inflorescences.

124

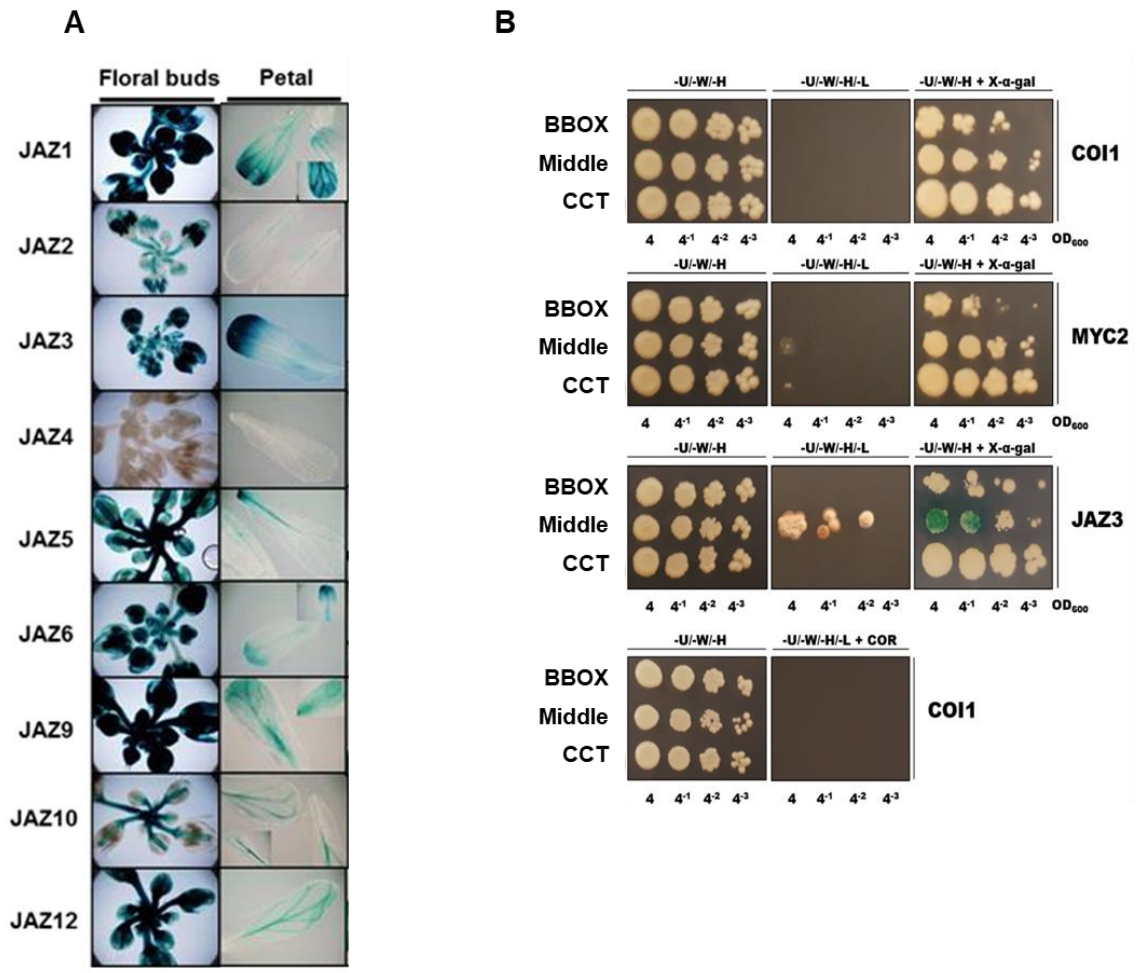

Supplementary Fig. S10 JAZs petal expression and Y2H interaction between CO-COI1, CO-MYC2 and CO-JAZ3 by Yeast Two Hybrid assays.

(A) GUS staining showing *pJAZs:GUS* expression in floral buds (left) and petals (right). Notice the coincide level of expression with the CO-JAZs interaction by BiFC in Sup FIG S11) **(B)** Interaction between different CO domains (BBOX, Middle and CCT), COI1, MYC2 and JAZ3 in Y2H assays in different selective media. COR: coronatine. Pictures show 3-day-old colonies. Left panels show growth controls, middle panels show growth assays, right most panels show the X-Gal staining with the positive result colonies stained in blue.

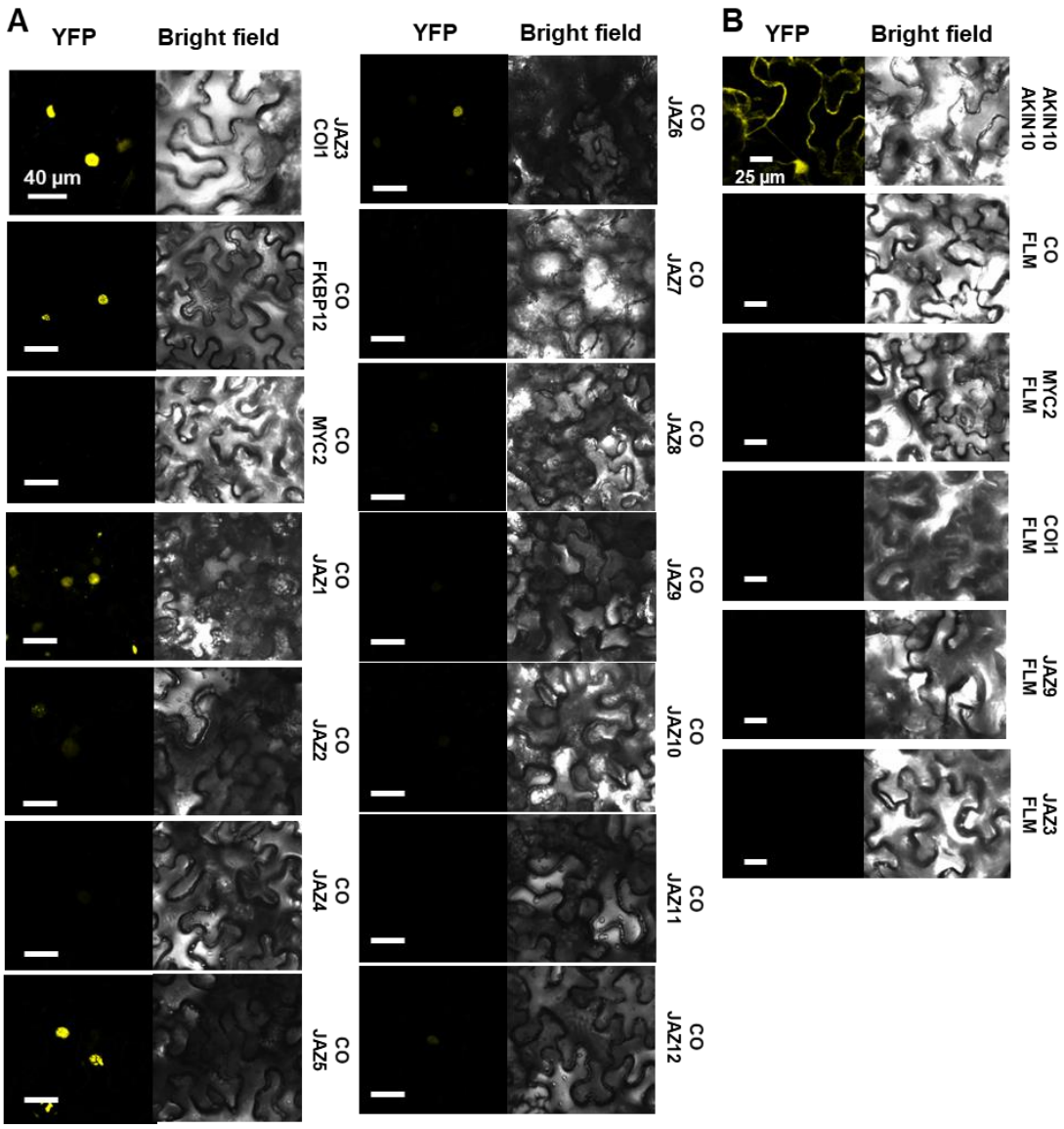

Supplementary Fig. S11 Interaction tests between CO-MYC2 and CO-JAZs by molecular complementation (BiFC) assays.

(A) Confocal microscope images of BiFC assays showing the interaction between YFC:CO and all YFN:JAZs and the lack of interaction between YFC:CO and YFN:MYC2 in agroinfiltrated *Nicotiana* leaves. JAZ3-COI and CO-FKBP12 are used as positive controls. Left panels, YFP fluorescence; right panels, bright field. Scale bars represent 40 μm **(B)** Confocal microscope images of BiFC assays showing a positive control interaction between YFN:AKIN10 and YFC:AKIN10, and negative controls using YFC:FLM with CO, MYC2, COI1, JAZ9 and JAZ3. Left panels, YFP fluorescence; right panels, bright field. Scale bars represent 25 μm.

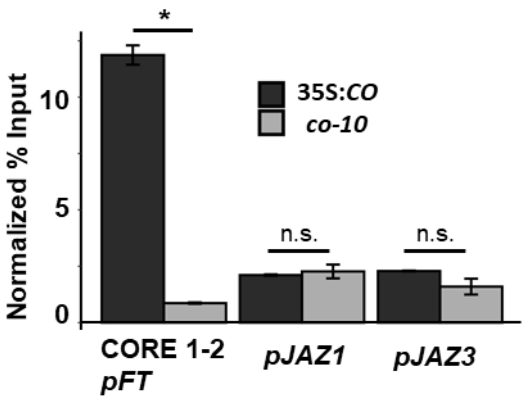

Supplementary Fig. S12 Occupancy of CO at *FT*, *JAZ1* and *JAZ3,* promoters.

The barplot shows the enrichment (% input) of amplicons located in *FT*, *JAZ1* and *JAZ3* promoters after ChIP experiments in 35S:*CO* and *co-10* plants. CORE1/2 site within *FT* promoter was used as positive control and putative CO binding sites in *JAZ1* and *JAZ3,* promoters were also tested. *ACT7* TSS locus was used to normalize each genomic region. Error bars indicate the standard errors for two biological replicates. Significant differences were evaluated using Student's test, * $p < 0.01$.

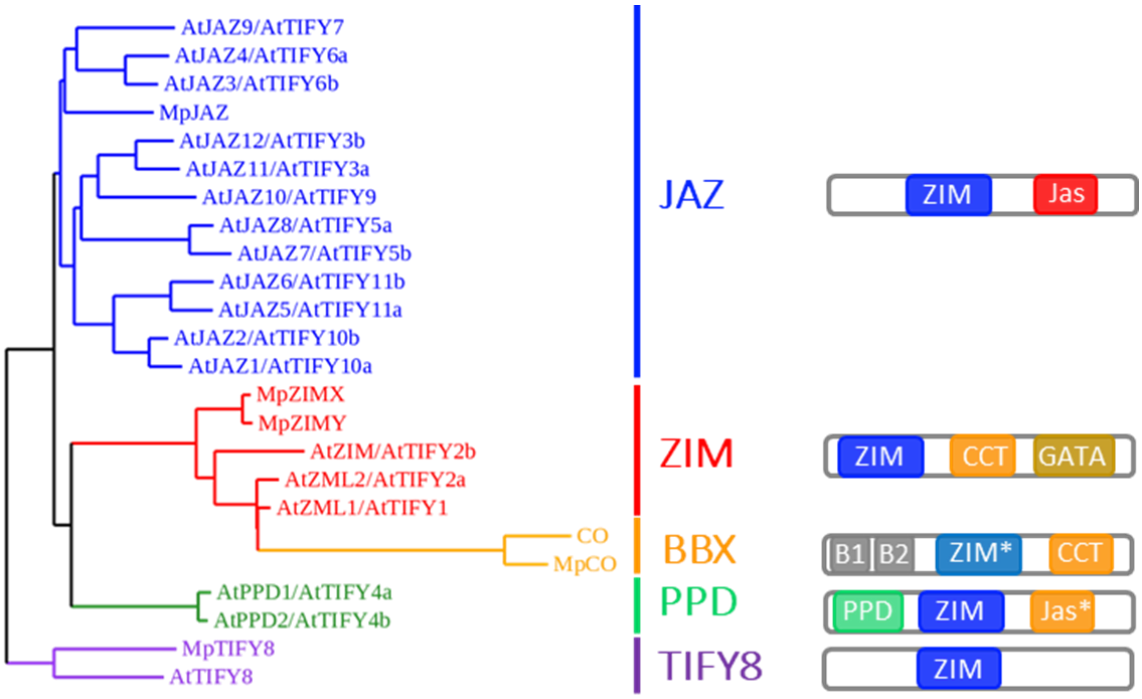

Supplementary Fig. S13 Phylogenetic analysis of ZIM-containing proteins.

Selected protein sequences of JAZ (blue), ZIM red), BBX (yellow), PPD (green) and TIFY8 (magenta) families were aligned using DiAling and PhyML apps and an unrooted phylogenetic tree created with Treeview app (left). The cartoons to the right show the protein structure including the common ZIM (ZIM-like domain or ZIM* in CO and MpCO, light blue) in deep blue, and specific domains: Jas (JAZ family, red), CCT (ZIM and BBX family, yellow); GATA (ZIM family, brown); B-boxes (BBX family, grey); PPD (PPD family, green) and Jas* (PPD family, yellow). At: *Arabidopsis thaliana*, Mp: *Marchantia polymorpha*.

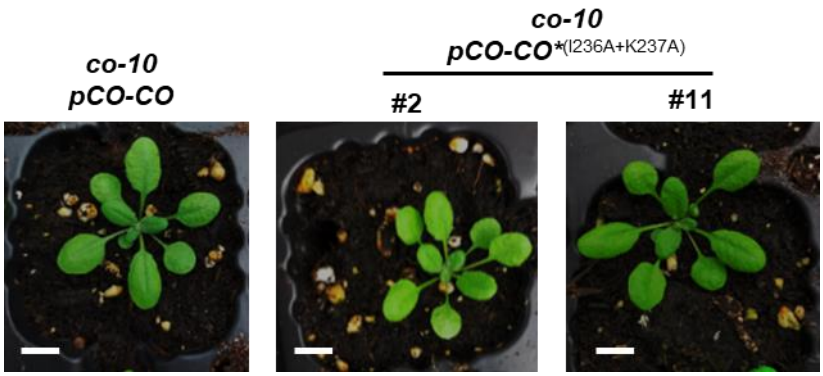

Supplementary Fig. S14 Flowering phenotype of *co-10* p*CO-CO (I236A+K237A)**

Pictures showing differences in flowering time between WT, *co-10*, *co-10* p*CO*:*CO* and two *co-10* independent lines expressing p*CO-CO*$^{*(I236A+K237A)}$. Scale bars represent 1 cm.

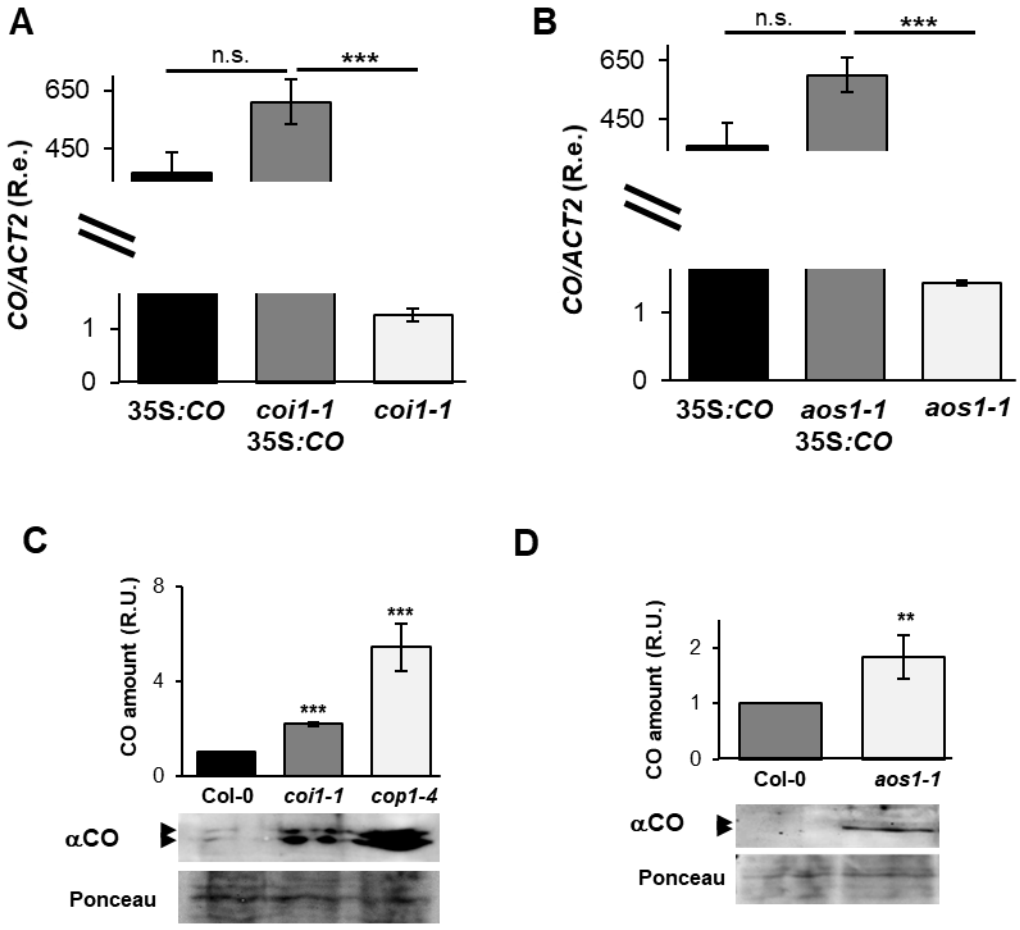

Supplementary Fig. S15 CO protein accumulation in *coi1-1* and *aos1-1* mutants.

(A) RT-qPCR analyses of the *CO* gene in *coi1-1* and *coi1-1* 35S:*CO* flowers, LD, ZT16. *ACT2* as control. Error bars, s.d. from three independent experiments **(B)** RT-qPCR analyses of the *CO* gene in *aos1-1* and *aos1-1* 35S:*CO* flowers, LD, ZT16. *ACT2* as control. Error bars, s.d. from three independent experiments **(C)** αCO immunoblot analysis of CO accumulation in WT, *coi1-1* and *cop1-4* flowers, stage 14, LD, ZT16 and protein quantification in three replicates ± s.d. Ponceau staining as loading control **(D)** αCO immunoblot analysis of CO accumulation in WT and *aos1-1* flowers, stage 14, LD, ZT16 and protein quantification in three replicates ± s.d. Ponceau staining as loading control.

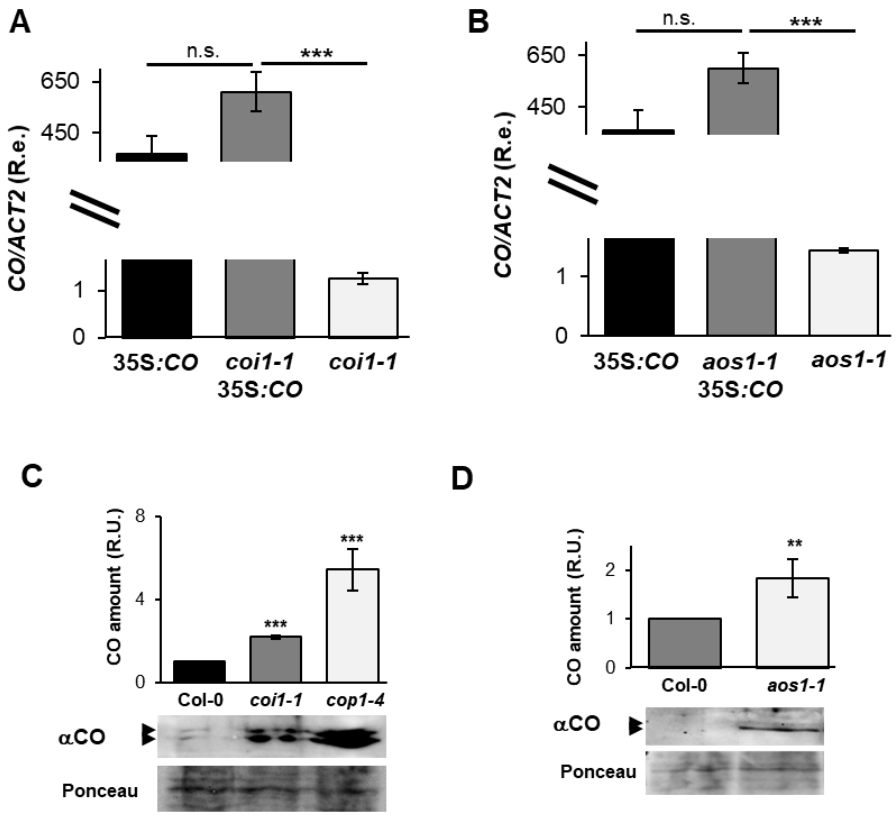

Supplementary Fig. S16. CO-JAZ3 interaction stabilizes the complex.

(A) Quantification of protein levels in three replicates (± s.d.) of HA:CO accumulation after co-incubation with *N. benthamiana* lysates expressing COI1 and COI1-JAZ3 for 30 min. Data is expressed as percentage of original protein at 0 min incubation time. Error bars show s.d. from three replicates **(B)** αHA Immunoblot analysis of FLM accumulation after co-incubation with *N. benthamiana* lysates expressing COI1-JAZ3 **(C)** RT-qPCR analyses of *CO* in WT, *co-10* p*CO*:*CO* and two *co-10* independent plant lines expressing p*CO-CO**$^{(I236A+K237A)}$ in flowers, LD, ZT16. *ACT2* as control. Error bars indicate s.d. from three independent experiments **(D)** Quantification of protein levels in three replicates (± s.d.) of experiment in Fig. 5G **(E)** RT-qPCR analyses of *COI1* (black), *CO* (dark grey) and *JAZ3* (light grey) in *Nicotiana* cells negative control (not agroinfiltrated), and expressing *YFN:COI1*, *HA:CO* and *YFN:JAZ3* constructs, respectively. Data is the media of two different experiments ± s.d.m. **(F)** Quantification of protein levels in three replicates (± s.d.) of experiment in Fig. 5H. **(G)** aGFP immunoblot analysis of JAZ3 accumulation in leaf extracts of *Nicotiana* agroinfiltrated with YFN:COI1/YFC:JAZ3 at 0 and 30 min incubation with (right panels) and without (left panels) CO and with (+) or without (-) MeJA (2 mM). Ponceau staining as loading control.

Table S1. Jasmonate, aging, senescence and flowering related genes up-regulated in 35S:*CO* seedlings vs WT.

ID	Name	GO term
Jasmonate related genes		
AT1G19640	JMT	jasmonic acid biosynthetic process/jasmonic acid mediated signaling pathway
AT5G42650	AOS CYP74A DDE2	jasmonic acid biosynthetic process/Response to jasmonic acid
AT1G19180	AtJAZ1 JAZ1 TIFY10A	jasmonic acid mediated signaling pathway/Response to jasmonic acid
AT2G34070	TBL37	jasmonic acid mediated signaling pathway
AT2G02990	ATRNS1 RNS1	jasmonic acid mediated signaling pathway/Aging
AT3G50480	HR4	Response to jasmonic acid
AT2G26690	AtNPF6.2 NPF6.2	Response to jasmonic acid
AT5G24780	ATVSP1 VSP1	Response to jasmonic acid
AT5G13220	JAS1 JAZ10 TIFY9	Response to jasmonic acid
AT4G23600	CORI3 JR2	Response to jasmonic acid
AT4G34710	ADC2 ATADC2 SPE2	Response to jasmonic acid
AT1G76930	ATEXT1 ATEXT4 EXT1 EXT4 ORG5	Response to jasmonic acid
AT5G67480	ATBT4 BT4	Response to jasmonic acid
AT5G24770	ATVSP2 VSP2	Response to jasmonic acid
AT3G09940	AtMDAR3 MDAR3	Response to jasmonic acid
AT4G26850	GGP VTC2	Response to jasmonic acid
AT3G15510	ANAC056 ATNAC2 NAC2 NARS1	Response to jasmonic acid
AT3G44860	FAMT	Response to jasmonic acid
AT2G39030	NATA1	Response to jasmonic acid
AT3G16470	AtJAC1 JAL35 JR1	Response to jasmonic acid
AT1G70700	JAZ9 TIFY7	Response to jasmonic acid
AT2G24850	TAT TAT3	Response to jasmonic acid
AT1G19570	ATDHAR1 DHAR1 DHAR5	Response to jasmonic acid
AT1G61120	GES TPS04 TPS4	Response to jasmonic acid
AT5G44420	LCR77 PDF1.2 PDF1.2A	Response to jasmonic acid
Aging and senescence related genes		
AT3G02150	A-PTF-1 bHLHb1 PTF1 TCP13 TFPD	Leaf senescence
AT1G66330		Leaf senescence
AT2G43570	CHI	Leaf senescence
AT1G17020	ATSRG1 SRG1	Leaf senescence
AT5G51720	At-NEET NEET	Leaf senescence
AT5G13170	AtSWEET15 SAG29 SWEET15	Leaf senescence/SAG (Senescence-associated gene)
AT2G29350	SAG13	Aging/SAG (Senescence-associated gene)
AT3G49620	DIN11	Aging
AT4G05320	UBI10 UBQ10	Aging
AT4G30270	MERI-5 MERI5B SEN4 XTH24	Aging
AT5G20230	ATBCB BCB SAG14	SAG (Senescence-associated gene)
Flowering related genes		
AT1G65480	FT RSB8	Flowering
AT2G45660	AGL20 ATSOC1 SOC1	Flowering
AT5G62430	CDF1	Flowering
AT3G47500	CDF3	Flowering
AT1G26790	CDF6	Flowering

Table S2. Primers used in this study.

Notes	Primer Name	Primer Sequence
For vector construction		
pCO(2Kb): *mGFP6*	pCO_FW	AAAAGCAGGCTTCTATTGTTACATATGATCT
	pCO_RV	AGAAAGCTGGGTCTTCACAAGAAAATTGAAGAGGAGA
For RT-qPCR		
CO	qCO_FW	CCCGAATTCATGTTGAAACAAGAGAGTAAC
	qCO_RV	GGGCTCGAGTCAGGAGCTGAAAGAGTTTCC
SAG13	qSAG13_FW	GTGCCAGAGACGAAACTC
	qSAG13_RV	GCTGTATACTCTGTGGT
SAG29	qSAG29_FW	GCCACCAGGGAGAAAAGG
	qSAG29_RV	CCACGAAATGTGTTACCATTAGAA
TOC1	qTOC1_FW	AACGGCGTGAATGTTGATTT
	qTOC1_RV	CGGTTCTCCTCTTCTTCTTCTTC
HY5	qHY5_FW	GCTGAAGAGGTTGTTGAGGA
	qHY5_RV	TCTCCAAGTCTTTCACTCTGTTT
PRR7	qPRR7_FW	GGAAGTGGTAGCGGAAACTTGG
	qPRR7_RV	CGTACCTTCTTTCGGAAGCACC
LEA3	qLEA3_FW	CCATGGGTTCCAGATCCTAAA
	qLEA3_RV	TGCTTGTTGTTCAAGAGAATAGC
CCA1	qCCA1_FW	TTTTAAACCATACAAAAGATGTTCCATGGAAGC
	qCCA1_RV	GGAAGCTTGAGTTTCCAACCG
UBQ10	qUBQ10_FW	GAAGTTCAATGTTTCGTTTCATGT
	qUBQ10_RV	GGATTATACAAGGCCCCAAAA
ACT2	qACT2_FW	GTAACATTGTGCTCAGTGGTGG
	qACT2_RV	CTCGGCCTTGGAGATCCACATC

Notes	Primer Name	Primer Sequence
For ChIP-QPCR		
CORE1-2 site	CORE_pFT_FW	GTGGCTACCAAGTGGGAGAT
	CORE_pFT_RV	TAACTCGGGTCGGTGAAATC
pJAZ1 site	pJAZ1_FW	AGCTTTGTTATATTGGAGGTAGGA
	pJAZ1_FW	TTGTCACGAGAGGGAGAAATG
pJAZ3 site	pJAZ3_FW	GCTTCGCATCTCGTGAATCAT
	pJAZ3_FW	GCAGTGTGTGGCGTTTCT
ACT7 TSS	ACT7_TSS_FW	GCGATGTTTGAGTTTCAATAAACGCTGC
	ACT7_TSS_FW	CTCACCTTCACCATTCCAGTTCCA
For Yeast Two Hybrid		
CO BBOX DNA cloning	YTH_BBOX_FW	ATGTTGAAACAAGAGAGTAAC
	YTH_BBOX_RV	TCAGGAGCTGAAAGAGTTTCC
CO Middle DNA cloning	YTH_Middle_FW	ATGACCACTACTCACCACCAA
	YTH_Middle_RV	TCATGGACTGAGTTGTGTTAC
CO CCT DNA cloning	YTH_CCT_FW	CCCGAATTCATGATAACAGTAACACAACTC
	YTH_CCT_RV	GGGCTCGAGTCAGAATGAAGGAACAATCCC
COI1 DNA cloning	YTH_COI1_FW	CCCCCATGGATGGAGGATCCTGATATCAG
	YTH_COI1_RV	CCCGTCGACTCATATTGGCTCCTTCAGGACTC
MYC2 DNA cloning	YTH_MYC2_FW	CCCAGATCTATGACTGATTACCGGCTACAACC
	YTH_MYC2_RV	CCCCCATGGTTAACCGATTTTTGAAATCAAACTTGC
JAZ9 DNA cloning	YTH_JAZ9_FW	CCCGAATTCATGGAAAGAGATTTTCTGGGTTTGAG
	YTH_JAZ9_RV	CCCGGATCCTTATGTAGGAGAAGTAGAAGAGTAATTC
JAZ3 DNA cloning	YTH_JAZ3_FW	CCCGAATTCATGGAGAGAGATTTTCTCGGGTTG
	YTH_JAZ3_RV	CCCCTCGAGTTAGGTTGCAGAGCTGAGAGAAGAAC
For site-directed mutagenesis		
CO I236A K237A*	mutpNIKYCO_FW	GAATTTTCAGTTCAAT**GC**C**GC**ATATGGCTCCTCAG
	mutpNIKYCO_RV	CTGAGGAGCCATAT**GC**G**GC**ATTGAACTGAAAATTC

Table S3. Vectors used in this study.

Vector name	Source
For plant transformation	
pCO(2Kb)*:mGFP6*	This study
pCO(2Kb)*:CO*	This study
pCO(2Kb):CO$^{*(I236A+K237A)}$	This study
For BiFC assay	
YFC:AKIN10	Ferrando et al., 2001
YFN:AKIN10	Ferrando et al., 2001
YFC:FLM	Serrano-Bueno et al., 2020
YFN:FLM	Serrano-Bueno et al., 2020
YFC:CO	Serrano-Bueno et al., 2020
YFN:CO	Serrano-Bueno et al., 2020
YFC:COI1	This study
YFN:COI1	This study
YFC:MYC2	This study
YFN:MYC2	This study
YFC:JAZ1	Chini et al., 2009
YFN:JAZ1	Chini et al., 2009
YFC:JAZ2	Chini et al., 2009
YFN:JAZ2	Chini et al., 2009
YFC:JAZ3	Chini et al., 2009
YFN:JAZ3	Chini et al., 2009
YFC:JAZ4	Chini et al., 2009
YFN:JAZ4	Chini et al., 2009
YFC:JAZ5	Chini et al., 2009
YFN:JAZ5	Chini et al., 2009
YFC:JAZ6	Chini et al., 2009
YFN:JAZ6	Chini et al., 2009
YFC:JAZ7	Chini et al., 2009
YFN:JAZ7	Chini et al., 2009
YFC:JAZ8	Chini et al., 2009
YFN:JAZ8	Chini et al., 2009
YFC:JAZ9	Chini et al., 2009
YFN:JAZ9	Chini et al., 2009
YFC:JAZ10	Chini et al., 2009
YFN:JAZ10	Chini et al., 2009
YFC:JAZ11	Chini et al., 2009
YFN:JAZ11	Chini et al., 2009
YFN:JAZ12	Chini et al., 2009
YFN:JAZ12	Chini et al., 2009

For Yeast Two Hybrid assay	
BD-CO-BBox	Serrano-Bueno et al., 2020
BD-CO-Middle	Serrano-Bueno et al., 2020
BD-CO-CCT	Serrano-Bueno et al., 2020
BD-CO$^{*(I236A+K237A)}$*-Middle*	This study
AD-COI1	This study
AD-MYC2	This study
AD-JAZ9	This study
AD-JAZ3	This study
For FRET assay	
CFP-CO	This study
CFP-HY5	This study
YFP-FLM	This study
For CO degradation assay	
HA-CO	This study
HA-FLM	This study